Research Square

Preprints are preliminary reports that have not undergone peer review.
They should not be considered conclusive, used to inform clinical practice,
or referenced by the media as validated information.

PICALM regulates a human microglial antigen presentation program in Alzheimer's disease

Bart De Strooper

bart.destrooper@kuleuven.be

KU Leuven

Sarah Borrie

VIB/KU Leuven Center for Brain & Disease Research https://orcid.org/0000-0002-6880-772X

Emanuela Pasciuto

VIB/UAntwerpen Center for Molecular Neurology

Laura Van Moortel

Department of Biomolecular Medicine, Ghent University, Ghent, Belgium.

Patrick Willems

Department of Biomolecular Medicine, Ghent University, Ghent, Belgium.

Daan Moechars

VIB KU Leuven

Nicola Thrupp

Department of Neurosciences and Leuven Brain Institute, KU Leuven, Leuven, Belgium

Pierre Bourdely

VIB/KU Leuven Center for Cancer Biology

An Snellinx

KU Leuven

Dries T'Syen

Department of Neurosciences and Leuven Brain Institute, KU Leuven, Leuven, Belgium

Ruoxin Li

Department of Biomedical Sciences, University of Antwerp, Antwerp, Belgium.

Amy Lloyd

University of Dundee https://orcid.org/0000-0002-1168-5370

Bethany Geary

University of Dundee

Hanne De Baene

Department of Neurosciences and Leuven Brain Institute, KU Leuven, Leuven, Belgium
https://orcid.org/0009-0003-3036-9538

Giulia Albertini

Department of Neurosciences and Leuven Brain Institute, KU Leuven, Leuven, Belgium

Daniel Álvarez Sirvent
Department of Clinical Genetics, VU University Medical Centre, Amsterdam, The Netherlands
Nienke Mekkes
Department of Biomedical Sciences, University of Groningen, University Medical Center Groningen, Groningen, The Netherlands
Inge Holtman
Department of Biomedical Sciences, University of Groningen, University Medical Center Groningen, Groningen, The Netherlands
Henne Holstege
Department of Clinical Genetics, VU University Medical Centre, Amsterdam, The Netherlands
Valeriya Malysheva
VIB Center for Molecular Neurology https://orcid.org/0000-0002-0919-7845
Massimiliano Mazzone
KU Leuven/VIB https://orcid.org/0000-0001-8824-4015
Francis Impens
Department of Biomolecular Medicine, Ghent University, Ghent, Belgium. https://orcid.org/0000-0003-2886-9616
Mark Fiers
VIB/KU Leuven Center for Brain & Disease Research https://orcid.org/0000-0001-5694-2409
Annerieke Sierksma
VIB Center for the Biology of Disease, Leuven, Belgium Center for Human Genetics, Universitaire ziekenhuizen and LIND, KU, Leuven, Belgium. https://orcid.org/0000-0001-9233-972X

Biological Sciences - Article

Keywords:

Posted Date: June 9th, 2026

DOI: https://doi.org/10.21203/rs.3.rs-9701645/v1

License: This work is licensed under a Creative Commons Attribution 4.0 International License.
Read Full License

Additional Declarations: Yes there is potential Competing Interest. B.D.S. has been a consultant for Eli Lilly, Biogen, Janssen Pharmaceutica, Eisai, AbbVie and other companies and is now consultant to Muna Therapeutics. B.D.S is a scientific founder of Augustine Therapeutics and a scientific founder and stockholder of Muna Therapeutics. B.D.S. is also a member of the scientific advisory board of Cell. M.F. is a consultant to Muna Therapeutics.

PICALM regulates a human microglial antigen presentation program in Alzheimer's disease

Sarah C. Borrie[1,2], Emanuela Pasciuto[1,2,3,4], Laura Van Moortel[5,6], Patrick Willems[5,6], Daan Moechars[1,2], Nicola Thrupp[1,2], Pierre Bourdely[7,8], An Snellinx[1,2], Dries T'Syen[1,2], Ruoxin Li [3,4], Amy F. Lloyd[9], Bethany Geary[10], Hanne De Baene[1,2], Giulia Albertini[1,2], Daniel Álvarez Sirvent[11], Nienke Mekkes[12], Inge R. Holtman[12,13], The Netherlands Brain Bank**, Henne Holstege[1,2,11,14], Valeriya Malysheva[3,4,15], Massimiliano Mazzone[7,8], Francis Impens[5,6], Mark Fiers[1,2,16,17], Annerieke Sierksma[1,2]*, Bart De Strooper[1,2,17]*

1) Department of Neurosciences and Leuven Brain Institute, KU Leuven, Leuven, Belgium
2) Center for Neuroscience Leuven, Flanders Institute for Biotechnology (VIB), Leuven, Belgium
3) Center for Molecular Neurology, Flanders Institute for Biotechnology (VIB), Antwerp, Belgium.
4) Department of Biomedical Sciences, University of Antwerp, Antwerp, Belgium.
5) Department of Biomolecular Medicine, Ghent University, Ghent, Belgium
6) VIB Center for Medical Biotechnology, VIB, Ghent, Belgium
7) Center for Cancer Biology, VIB, Leuven, Belgium.
8) Department of Oncology, KU Leuven, Leuven, Belgium.
9) Division of Cell Signaling and Immunology, School of Life Sciences, University of Dundee, Dundee, UK
10) Medical Research Council (MRC) Protein Phosphorylation and Ubiquitylation Unit, School of Life Sciences, University of Dundee, Dundee, UK.
11) Genomics of Neurodegenerative Diseases and Aging, Human Genetics, Vrije Universiteit Amsterdam, Amsterdam UMC, Amsterdam, The Netherlands
12) Department of Biomedical Sciences, University of Groningen, University Medical Center Groningen, Groningen, The Netherlands
13) The Netherlands Brain Bank, Netherlands Institute for Neuroscience, Amsterdam, The Netherlands
14) Alzheimer Centre, Department of Neurology, VU University Medical Centre, Amsterdam, The Netherlands
15) VIB Center for AI and Computational Biology, VIB, Leuven, Belgium
16) Department of Human Genetics, KU Leuven, Leuven, Belgium
17) UK Dementia Research Institute at UCL, University College London, London, UK

* corresponding authors
** Consortium order list for The Netherlands Brain Bank: Inge R. Holtman[12, 13], Dennis Wever[13], Inge Huitinga[13]

Email to: b.strooper@ukdri.ac.uk, annerieke.sierksma@kuleuven.be

Abstract

Microglia surrounding amyloid plaques in Alzheimer's disease (AD) strongly upregulate HLA class II genes, but whether this transcriptional state reflects antigen presentation, and how it relates to genetic risk, remains unclear. Here we identify a broad repertoire of endogenous HLA-bound peptides in human brain extracts from individuals with and without AD. Using human microglia xenografts isolated after exposure to plaques, we show that amyloid pathology induces an HLA-expressing microglial state that presents a similarly diverse spectrum of peptide antigens. This response was accompanied by increased expression of costimulatory and coinhibitory molecules, supporting a transition towards an antigen

presenting microglial state. Loss of *PICALM*, a major AD risk gene involved in endolysosomal trafficking, markedly amplified the microglial HLA response to amyloid pathology, and was associated with increased intracellular Aβ accumulation and modulation of immune regulatory proteins. These findings identify amyloid pathology as a driver of antigen presentation in human microglia and establish endolysosomal trafficking as a genetic regulator of this disease-associated immune state. Unexpectedly, the microglial immunopeptidome was not dominated by Aβ or tau, suggesting that amyloid plaques act less as a dominant antigenic source and more as a trigger of broader self-antigen presentation in the CNS by microglia.

Introduction

Microglia, the resident immune cells of the brain, are central regulators of the cellular response to Aβ-pathology in Alzheimer's disease (AD)[1–5]. They mobilize innate immune functions, including phagocytosis and activation through pattern-recognition receptors[6]. By contrast, the possibility that microglia also engage pathways classically associated with adaptive immunity has been less extensively explored. It has long been recognized that microglia surrounding amyloid plaques express human leukocyte antigen (HLA) class II proteins[7–12]. More recent single cell sequencing studies have confirmed that microglia respond to amyloid plaques with robust upregulation of HLA class II genes in AD patients[13–16] and in human microglia xenografted into mouse models of amyloid pathology[5,17–20].

The critical question is whether this HLA response reflects antigen presentation by parenchymal microglia. Antigen presenting cells must generate peptides, load them onto HLA complexes, traffic these complexes through the endolysosomal system to the cell surface, and present them in a molecular context that enables T cell engagement. In HLA class I presentation, peptides are generally derived from cytosolic proteasomal processing and presented to $CD8^+$ T cells. In HLA class II presentation, peptides are generated in the endolysosomal compartment from extracellular or phagocytosed antigens and presented to $CD4^+$ T cells[21]. Antigen presentation is further shaped by the co-expression of costimulatory and coinhibitory surface proteins and by cytokine signalling, which together form the antigen presenting side of the immune synapse and determine the functional outcome of T cell engagement[22,23].

Under homeostatic conditions, HLA class II antigen presentation in the central nervous system (CNS) occurs mainly at border compartments such as the dura and meninges, where dendritic cells and macrophages contribute to immune surveillance and immune tolerance[24]. Mouse microglia can upregulate HLA class II in response to interferon-γ and can engage T cells under conditions in which the blood brain barrier is damaged[25,26]. In human AD brain, however, T cell infiltration into the parenchyma appears limited[27,28], and, when present, has been linked particularly to cerebral amyloid angiopathy[29]. It therefore remains unclear whether the HLA response in parenchymal microglia around amyloid plaques represents a genuine antigen presentation program. The HLA response of human microglia must be considered in the context of brain immune privilege, which is now understood to be regulated rather than absolute. Recent work in the mouse CNS indicates that MHC class II presentation of brain specific antigens, including myelin basic protein, at the brain borders may promote immune tolerance, a central feature of CNS immune regulation[24]. Whether a related principle applies to amyloid plaques associated microglia is AD remains unknown. A key unresolved issue is therefore the identity of the antigens presented by microglia in the AD brain. Peripheral T cells can mount responses to Aβ and tau peptides[30–33], and specific HLA class II molecules have been linked to the presentation of these AD related antigens[34–36]. However, the endogenous HLA-bound peptide repertoire presented by microglia in Alzheimer's disease has not been defined.

A further way to establish the disease relevance of a microglial cell state is to determine whether it is influenced by genetic risk for AD. In a related study, we showed that polygenic risk for AD correlates with the microglial HLA response[37]. Here we focus on *PICALM*, an AD risk gene implicated in endolysosomal functions[6]. Genetic variants at the *PICALM* locus are associated with late onset AD[38] and map to microglia enhancer regions[39]. PICALM regulates clathrin-mediated endocytosis, autophagy and lysosomal degradation[40–42], processes that are directly relevant to antigen processing and HLA trafficking.

In this study we first show that HLA class I and class II immunopeptidomes can be recovered from human AD brain and are not dominated by Aβ- or Tau-derived peptides, but comprise a broad repertoire of peptides derived from brain proteins, including myelin basic protein. Because bulk brain extracts do not identify the presenting cell type, we used human microglia xenografts in amyloid plaque-bearing mouse brain and took advantage of human-specific HLA immunoprecipitation to recover HLA-bound peptides from xenografted brains and from isolated human microglia. These experiments demonstrate that parenchymal human microglia exposed to amyloid plaques present HLA-bound peptides *in vivo* and acquire additional features of the antigen presenting side of the immune synapse[23]. Finally, we show that loss of *PICALM* amplifies this response, linking amyloid-induced microglial antigen presentation to a major AD risk gene. Together, these findings identify antigen presentation as an intrinsic response of human microglia to amyloid plaque pathology and establish endolysosomal trafficking as a genetic regulator of this AD-associated immune state.

Results

The human parenchymal CNS immunopeptidome in Alzheimer's disease

We sequentially recovered high quality HLA class I-bound (HLA-I) and HLA class II-bound (HLA-II) immunopeptides from superior frontal gyrus samples of three individuals with AD and three age-matched non-AD controls (Figure 1A). Peptide-binding predictions based on each individual's HLA haplotype (Supplementary Table 1) confirmed the expected features of the recovered immunopeptidomes. HLA-I peptides showed the characteristic predominance of 9-mer (Figure 1B), whereas HLA-II peptides spanned a broader length range peaking at 14- to 16-amino acids (Figure 1C). Across samples, we identified between 137 and 636 HLA class I peptides per sample, mapping to 636 unique source proteins in total (Supplementary Table 2) and between 654 and 1039 HLA class II peptides per sample mapping to 409 unique source proteins in total (Supplementary Table 3).

We first examined the HLA class II immunopeptidome, because HLA class II presentation is the canonical pathway by which phagocytosed or extracellular antigens are processed in the endolysosomal system and presented to CD4+ T cells. Across both AD and control samples, the human brain HLA class II immunopeptidome was strongly enriched for peptides derived from myelin basic protein (MBP), an oligodendrocyte protein and major component of myelin (Figure 1D, Supplementary Table 4, Supplementary Table 5). MBP enrichment has also been observed in mouse CNS MHC class II immunopeptidome data[24], although that study included meningeal tissue, which was absent from our parenchymal samples. Other oligodendrocyte and myelin associated proteins, including TPPP and PLP1, were also represented among HLA class II bound peptides, indicating that myelin derived antigens constitute a prominent component of the human parenchymal HLA class II immunopeptidome.

The HLA class II immunopeptidome was not restricted to myelin proteins. Up to 200 unique source proteins were detected per sample, and several abundant HLA class II peptides were shared between AD and control samples, including peptides derived from HMGN2 and SPARCL1, as well as the cytoskeletal proteins MAPT (Figure 1D) and ACTN4 (Supplementary

Table 3). Overall, 6.5% of HLA class II peptides mapped to brain-specific proteins[43]. In addition to oligodendrocyte and myelin derived peptides, GFAP was detected in all samples. Peptides mapping to synaptic proteins, including NRXN1, NRXN2, NRGN, SLC1A2 and SYN1, and to neuronal proteins, including CNTN2, CEND1 and MAP1A, were also prominent (Supplementary Table 6). Thus, the human parenchymal HLA class II immunopeptidome contains a broad repertoire of brain derived peptides, including synaptic peptides that were not reported in mouse CNS[24].

We next examined the HLA class I immunopeptidome. Although HLA class I peptides are typically generated from cytosolic proteins through proteasomal processing, MBP derived peptides were also enriched among HLA class I bound peptides in human brain (Figure 1D, Supplementary Table 4, Supplementary Table 5). This observation is consistent with cross presentation, a process by which exogenous antigens that are classically loaded onto HLA class II complexes can also enter the HLA class I pathway and thereby engage CD8+ T cells[44]. Cross presentation is well established in dendritic cells, where it can direct immune responses towards immunity or cross cross-tolerance[45], but it is much less studied in other immune cells[46].

To further assess the CNS origin of the HLA class I peptide repertoire, we restricted the HLA class I dataset to brain enriched proteins[43]. In total, 2.4% of HLA class I peptides were uniquely brain enriched, mapping to 15 source proteins. These included oligodendrocyte derived peptides from MAG and OPALIN, astrocyte associated peptides from GFAP, PEA15 and S100B, and neuronal peptides from MTURN, CNTN2, CTNND2, SEPTIN8, CACNG8 and TBR1 (Supplementary Table 6). Thus, HLA class I complexes recovered from human parenchymal brain extracts carry peptides derived from multiple CNS resident cell types, including myelin, astrocytic and neuronal proteins.

We then asked whether the AD immunopeptidome was dominated by the canonical disease proteins Aβ and tau. Although this bulk brain dataset is descriptive and does not identify the presenting cell type, more HLA class II peptides were detected in AD samples than in control samples (Supplemental Figure 1A,B). Several proteins linked to AD were represented by HLA class II peptides in all AD samples but not in controls, including calsyntenin 1 (CLSTN1), a regulator of APP production, and complement C4 (Supplementary Table 5). However, peptides derived from Aβ and tau were not selectively enriched in the AD immunopeptidome. The number of MAPT derived peptides did not differ between AD and control samples (Supplementary Table 5), despite the central role of tau aggregation in AD. Only a single immunopeptide mapping to the Aβ sequence DAEFRHDSGYEVH was detected, in one AD individual (Supplemental Figure 1D, highlighted in yellow in Supplementary Table 3). This was not explained by lack of Aβ protein in the tissue, as bulk proteomics performed on the same samples showed increased intensity of Aβ protein in AD relative to control samples (Supplemental Figure 1C). Thus, the HLA bound peptide repertoire recovered from human AD brain is not dominated by Aβ and tau, but instead reflects a broad and diverse repertoire of brain derived peptides.

Xenografted human microglia upregulate an APC module in response to amyloid pathology

Our human brain data identified a broad parenchymal HLA bound peptide repertoire, but frozen human brain tissue likely reflects contributions from multiple cell types, including both professional and non-professional APCs. The detection of HLA-II peptides derived from oligodendrocytes, astrocytes, and neurons indicates that CNS antigens are being presented by cells other than their cell of origin. Given their role as the principal phagocytes of the brain parenchyma, microglia are a plausible candidate source of this antigen presentation. To test

this directly, we turned to the *App*^{NLGF} AD mouse model xenografted with human microglia, which exposes engrafted human microglia to high levels of amyloid pathology[5,17,47].

We first asked whether uptake of Aβ-rich plaque material by human microglia is linked to induction of the HLA class II response. We labelled fibrillar Aβ plaques in *App*^{NLGF} xenografts *in vivo* with methoxy-X04, a beta-sheet binding dye, and used FACS to isolate human microglia that had taken up methoxy-X04 positive material over a 3 hour period together with the complementary methoxy-X04 negative population (Figure 2A). Bulk RNA sequencing and differential expression analysis showed that methoxy X04 positive microglia upregulated *HLA-DRA*, *HLA-DRP1 and HLA-DRB1* together with DAM and phagocytosis-related genes such as *GPNMB, CD9*, *APOE, NPC2, LPL* and *TYROBP* (Figure 2B). These findings link direct uptake of Aβ-rich plaque material to a marked HLA response in human microglia, supporting the idea that plaque-associated phagocytosis is a key driver of antigen presentation in AD.

Effective antigen presentation requires more than HLA expression alone. It depends on coordinated expression of the invariant chain CD74, which supports HLA class II assembly and trafficking, costimulatory and coinhibitory ligands that shape T cell engagement and CD83 which regulates surface expression of HLA-DR and other immune ligands[48]. To determine whether amyloid pathology also induces this broader machinery in human microglia, we performed CITE-seq profiling on human microglia isolated from *App*^{NLGF} xenografts and from *App*^{Hu} xenografts, which lack amyloid pathology[49], and assessed the expression of proteins associated with professional antigen presentation[23] (Figure 2C-F). We curated an APC protein expression module based on literature[23], restricted to proteins well expressed in our dataset and covering key APC functions: HLA-DR, CD74, CD83, canonical costimulatory ligands CD40, CD70, CD80, CD86, CD276, CD275/ICOSLG and coinhibitory ligands CD274/PD-L1 and CD273/PD-L2. When projected onto UMAP space, these proteins individually localised predominantly to DAM, HLA and IRM clusters, consistent with previous annotations[5] (Figure 2C-D). Human microglia exposed to amyloid pathology showed coordinated induction of this APC protein module, with significant enrichment in the *App*^{NLGF} condition relative to *App*^{Hu} controls (Figure E-F). Thus, amyloid pathology drives the transition towards a coordinated APC-associated program in human microglia, that encompasses HLA induction together with costimulatory and coinhibitory components of the antigen presenting side of the immune synapse.

Human xenografted microglia present HLA-bound immunopeptides in the context of Aβ pathology

To determine whether the human CNS immunopeptidome includes peptide presentation by microglia, we tested directly whether human microglia present HLA bound peptides *in vivo*. We applied our immunopeptidomic workflow to whole brain lysate from amyloid plaque-bearing *App*^{NLGF} mice xenografted with H9-derived human microglia (Figure 3). Because the antibodies used for immunoprecipitation specifically recognise *human* HLA class I and HLA class II complexes, the recovered peptide HLA complexes must originate from the engrafted human cells. We further validated this approach by performing the same analysis on FACS-isolated human microglia from the same experimental condition. In whole brain lysate from xenografted *App*^{NLGF}-mice, we detected 1647 distinct 8-12-mer peptides bound to HLA class I complexes, with a sharp peak at 9-mer. In FACS-isolated human microglia we detected 1490 HLA class I bound peptides with a similar length distribution (Figure 3A, Supplementary Tables 8 &9). For HLA class II, we detected 247 distinct predicted HLA-II binding peptides in whole brain lysates and 182 in isolated human microglia, with the expected peak at 14- to 16-mer (Figure 3F, Supplementary Tables 10 &11). Peptides recovered from whole xenografted brain lysate, which model the human brain tissue workflow used in Figure 1, overlapped with those recovered from isolated human microglia with 1212 HLA class I peptides and 64 HLA class II peptides detected

in common (Figure 3A,F). This concordance indicates that the workflow yields reproducible peptide identifications, and supports the conclusion that the human HLA peptide complexes recovered from whole xenografted brain lysates originate from engrafted human microglia.

Unsupervised Gibbs clustering and HLA predictions showed a strong imprint of H9 HLA haplotype, including HLA-A*03:01, HLA-B*35:03 and HLA-B*44:02 on the immunopeptidome of the xenografted human microglia (Figure 3D-E, Supplemental Table 1). A substantial fraction of peptides mapped to both human and mouse protein sequences for HLA class I and class II complexes (Figure 3B, G), reflecting sequence conservation between the two species homology for those proteins. Pathway analysis of HLA-I peptide source proteins revealed enrichment for metabolic and RNA related processes, together with proteins associated with viral response pathways (Figure 3C). A subset of mouse-specific peptides was bound to human HLA-I complexes (Figure 3B). Because these peptides derive from the mouse CNS environment but were recovered on human HLA complexes, this finding shows that xenografted human microglia can acquire exogenous CNS antigens and present them through HLA class I *in vivo*. This is consistent with cross-presentation (Figure 1), and provides direct evidence that human microglia can mediate this process in the brain. As expected, the HLA class II immunopeptidome of xenografted human microglia included both mouse and human peptides, consistent with the fact that engrafted human microglia survey a mouse brain environment and present peptides derived from both neighbouring mouse cells as well as from other human microglia (Figure 3G).

We next asked whether the xenograft immunopeptidome recapitulated features of the human brain immunopeptidome. Among source proteins represented by HLA bound peptides, 61 HLA-I source proteins and 41 HLA-II source proteins overlapped between xenografted human microglia and the corresponding human brain immunopeptidomes, including MBP and MAPT. This indicates that the xenograft model recapitulates key features of the human CNS immunopeptidome. Notably, even in this high amyloid context[50], no peptides mapping to the Aβ sequence were detected. Together, these findings show that human microglia are a direct source of CNS HLA peptide presentation *in vivo* and suggest that even under conditions of substantial amyloid burden, the microglial immunopeptidome is not dominated by Aβ-derived peptides.

The endolysosomal AD risk gene *PICALM* modulates antigen presentation associated phenotypes

We previously found that the extent to which amyloid exposure induces HLA class II gene expression in human microglia correlates with individual AD polygenic risk score[37]. This suggested that the antigen presentation associated microglia phenotype is regulated, at least in part, by AD genetics. Although AD risk genes converge strongly on the endolysosomal pathway[6], which is also involved in canonical HLA class II peptide presentation, whether this pathway regulates HLA class II antigen presentation programs in AD microglia has not been explored. *PICALM* is one the most significant late onset AD risk genes[38], and has been linked to defective microglia lysosomal degradation in AD[40]. We therefore asked whether disruption of endolysosomal function through loss of *PICALM* alters the transition of human microglia towards an antigen presentation associated state.

We generated two independent $PICALM^{-/-}$ H9 ESC clones, differentiated them into microglia precursors and grafted them into amyloid-bearing App^{NLGF} or non-amyloid $App^{Hu/Hu}$ mice (Figure 4A, Supplemental Figure 2). After 6 months, human microglia were isolated for single cell transcriptomic analyses and data from both clones were merged for downstream analysis (Figure 4B). Across both amyloid and non-amyloid conditions, loss of *PICALM* induced a coherent transcriptional shift towards antigen presentation programs relative to H9 controls.

WGCNA identified modules (Supplementary Table 12) corresponding to HLA class II antigen presentation (purple module: *CD74, HLA-DRA, HLA-DRB1, HLA-DRB5)* and HLA-class I antigen presentation (darkgreen module: *B2M, HLA-A, HLA-B, HLA-C*), both of which were significantly upregulated in *PICALM*$^{-/-}$ microglia under amyloid and non-amyloid conditions (Fig 4C, D). Modules associated with the human DAM state (yellow module: *SPP1, CD9, APOC1, GPNMB*)[5] and innate immune activation (greenyellow module: *IL4I1, GBP1, IL1RN, CD48;* salmon module: *IL1A, ICAM1)* were also increased (Figure 4C-D).

Differential gene expression analysis of the single cell data confirmed broad upregulation of both HLA class I and class II transcripts in *PICALM* deficient microglia (Figure 4E,F), including *HLA-A, HLA-B, HLA-C, HLA-F, HLA-DQA1, HLA-DRB5, HLA-DQB1*, and *HLA-DRA* (Figure 4F, Supplementary Tables 13 &14). Many of these genes were already induced when *PICALM*$^{-/-}$ microglia were grafted in non-amyloid *App*^{Hu} control mice, including HLA class I genes (Figure 4F). Selected APC-associated genes were also upregulated in both conditions, including immune adhesion molecules *ICAM1* and *NECTIN2*, the pro-inflammatory chemokine *CXCL8*, and *CXCL12*, which can provide costimulatory signal for T cells[51] (Figure 4F). These data indicate that *PICALM* loss induces a basal HLA high state that is intrinsic to these microglia and is further amplified by amyloid exposure. In non-amyloid *App*^{Hu} mice, *PICALM*$^{-/-}$ microglia additionally displayed a pronounced type I interferon response marked by the induction of *IFI44, IFI44L, MX1, IFIT1, and ISG15* (Figure 4E). Pathway enrichment analyses highlighted terms related to antigen presentation and T cell activation, as well as endosome and phagocytosis pathways in *App*^{Hu} (Figure 4G-H).

Bulk proteomic profiling of FACS isolated microglia at 6 months confirmed these shifts at the protein level. In *App*^{Hu} mice, *PICALM*$^{-/-}$ microglia from clone 1 upregulated interferon related proteins, including IFI44L, OAS3, IFIT1, ISG15, together with lysosomal proteins such as ATP6V0D1, and CTSG (Figure 4I). This was consistent with immunohistochemical detection of increased IFITM3, a marker of interferon signaling, in the brains of these mice at 6 months (Supplementary Figure 3). In *App*^{NLGF} mice, *PICALM*$^{-/-}$ microglia showed strong induction of HLA class II proteins including HLA-DRA and HLA-DRB5 as well as lysosomal proteins such as NPC2 and PLIN2, relative to controls. Histology confirmed enhanced microglial HLA-DR staining in amyloid-rich regions (Figure 4J-K).

We next asked whether the HLA-high phenotype of *PICALM*$^{-/-}$ microglia was associated with an altered response to Aβ pathology. In 10 month old *App*^{NLGF} xenografts, fibrillar plaques were labelled *in vivo* with methoxy-X04 (Figure 2A), and intracellular Aβ accumulation in human microglia was quantified by flow cytometry. *PICALM*$^{-/-}$ microglia contained significantly higher levels of internalized Aβ than control microglia (Figure 5A-B), and the proportion of methoxy-X04-positive cells was also increased (Figure 5C). This difference was even more pronounced in the CD68-high hCD45 microglial subset, consistent with greater Aβ accumulation in actively phagocytic microglia (Figure 5D, E). The increased intracellular burden in *PICALM*$^{-/-}$ could reflect enhanced uptake, impaired degradation, or both. Because a loss of PICALM has been reported to impair phagocytic processing *in vitro*[40], our findings are consistent with defective Aβ clearance *in vivo*. Within the methoxy-XO4-positive subset, HLA-DR levels were higher in *PICALM*$^{-/-}$ than in control microglia (Figure 5F), indicating that the elevated HLA-state induced by *PICALM*$^{-/-}$ (Figure 4) is maintained and further enhanced in microglia that have accumulated plaque-derived material. These data suggest that *PICALM*$^{-/-}$ microglia encounter the amyloid environment from a higher basal immune activated HLA-state and further intensify this response as intracellular Aβ accumulates.

Finally, flow cytometry showed that increased surface HLA-DR and HLA-A/B/C expression in *PICALM*$^{-/-}$ microglia (Figure 5G,H) was accompanied by increased intensity of costimulatory molecules CD40, CD86 and CD80, as well as coinhibitory molecule PD-L1 (Figure 5 I-M).

Together, these finding show that loss of *PICALM* drives an intrinsic APC-associated phenotype in human microglia, characterised by coordinated upregulation of HLA class I and class II programs, accessory immune molecules, and interferon response genes, and that this phenotype is further amplified by exposure to Aβ pathology.

Discussion

Our study establishes three main points. First, the plaque associated HLA response of human microglia in AD is not merely a transcriptional marker of microglial activation, but is accompanied by HLA bound peptide presentation and by coordinated expression of costimulatory and coinhibitory molecules. Second, the endogenous HLA bound peptide repertoire in AD brain and plaque exposed human microglia is broad and is not dominated by Aβ or tau. Third, the strength of this program is genetically regulated by PICALM, linking endolysosomal trafficking, Aβ handling and AD risk to microglial communication with adaptive immunity. Together, these findings identify antigen presentation as an intrinsic human microglial response to amyloid pathology and place it within the genetic and cellular architecture of AD.

This conclusion changes the interpretation of a long standing neuropathological observation. Reactive microglia in AD have been known for decades to express HLA-DR and other HLA molecules[9,52,53], but these signals were generally interpreted as markers of activation or myeloid reactivity[54]. Our data show that this view is incomplete. In AD, HLA expression is plaque associated[5,20], strongly influenced by AD genetic risk[37], and occurs in cortical and hippocampal parenchyma where T cell infiltration is relatively limited[27–29]. The relevant biological question is therefore not simply whether microglia express HLA, but what they present, whether they acquire the accessory machinery required for T cell interaction, and why this program is induced in a brain environment with few local T cells. By combining direct HLA immunopeptidomics with protein level detection of costimulatory and coinhibitory molecules *in vivo*, and building on our recent observation that amyloid exposed human microglia can stimulate naïve T cells[37], we show that the plaque associated HLA response is part of a coordinated APC associated state.

A key enabling advance was the ability to recover high quality HLA class I and class II immunopeptidomes from limited human brain material and from sorted xenografted human microglia. Previous immunopeptidomic analyses of clinical human material were constrained by the requirement for large amounts of tissue or high cell numbers[55], and earlier CNS studies identified only limited peptide repertoires or focussed on specific HLA alleles[56]. Recent improvements in mass spectrometry sensitivity and peptide identification[57–60] allowed us to move beyond HLA expression and directly define HLA bound peptides in human AD brain. Importantly, the xenograft model then resolved the cellular source of these peptides. Because human specific HLA antibodies recover HLA complexes only from engrafted human cells in the mouse brain, and the peptide repertoire of whole xenografted brain lysates strongly overlapped with sorted human microglia, these data demonstrate that parenchymal human microglia are a direct source of CNS HLA-bound peptide presentation *in vivo*. This conclusion is supported by recent *in vitro* work showing that iPSC derived human microglia can present a broad peptide repertoire after interferon exposure[61], but our data place this capacity in the context of amyloid pathology in the living brain.

The most unexpected result is that amyloid pathology induces antigen presentation without making Aβ the dominant presented antigen. Prior work has focused mainly on whether Aβ or tau peptides can activate peripheral T cell response[30,31,34–36,62], often implying that antigen presentation in AD would primarily involve canonical disease proteins. Our unbiased approach argues against this simple model. In both human AD brain and xenografted human microglia,

HLA bound peptides comprised a broad repertoire of brain derived proteins. MBP and other myelin-associated proteins were prominent, together with peptides from cytoskeletal, extracellular, astrocytic, synaptic and neuronal proteins. This resembles recent work showing that murine CNS MHC-II presentation is enriched for endogenous self-peptides, particularly myelin-derived peptides[24] and is consistent with the high peptide heterogeneity reported in brain derived tumours such as glioblastoma[63,64]. Thus, amyloid exposure appears to act less as the dominant antigenic substrate and more as a local trigger that induces microglia to present a broad repertoire of CNS self peptides.

This broader repertoire reframes the potential function of antigen presentation in AD. One possibility is that plaque associated microglia promote T cell activation and contribute to neuroinflammation, particularly when costimulation is high and peripheral T cells have already been primed. Peripheral T cell activation has been reported during AD progression[29,31,65], and a model of tau-mediated neurodegeneration showed peripheral priming of $CD8^+$ T cells by brain-derived antigen[66]. Our finding that human microglia can present exogenous CNS derived peptides on HLA-I complexes also raises the possibility that cross presentation contributes to immune surveillance in AD[44,46]. However, the low abundance of T cells in AD parenchyma[27–29] and the broad self peptide repertoire also point to a regulatory function. Endogenous CNS-derived MHC-II peptides at brain border compartments can help preserve immune privilege by restraining self reactive T cell responses through coinhibitory pathways[24]. In AD models, plaque-associated microglia express immune regulatory molecules: CD28 upregulation in microglia has been linked to a suppressive microglial phenotype around amyloid plaques[67], checkpoint pathways such as PD1 to PDL1 signaling[68] and TIM-3[69] regulate microglial homeostasis, and PD1 positive CD8+ T cells have been reported to exert protective effects in AD models[70]. In this context, plaque associated microglial HLA upregulation may not primarily serve to present Aβ or tau as disease specific antigens, but may regulate T cell responses against self antigens in an inflamed CNS environment.

PICALM provides a genetic entry point into this biology. Loss of PICALM drove a cell-intrinsic increase in HLA class I and class II programs, costimulatory and coinhibitory molecules, and interferon-responsive genes, even in the absence of amyloid pathology. This phenotype was further amplified in amyloid-bearing brain, where PICALM-deficient microglia accumulated more intracellular Aβ, consistent with altered Aβ processing[40,42]. These findings fit with the broader view that AD risk genes expressed in microglia converge on endolysosomal function[5,20,71], but they extend that view by linking endolysosomal trafficking directly to an antigen presentation associated phenotype. PICALM loss therefore does not simply alter Aβ handling, it shifts the immune state from which microglia respond to amyloid pathology.

Together, our findings support a model in which amyloid plaques locally induce human microglia to enter an APC associated state, while endolysosomal AD risk genes tune the intensity and possibly the outcome of this response. The central implication is that antigen presentation in AD should not be viewed only as a mechanism for Aβ or tau directed immune attack. It may instead represent a broader system for surveying, presenting and regulating CNS self antigens during chronic tissue stress. Whether this response is protective, maladaptive or context dependent will likely depend on the peptide repertoire, the cytokine milieu, the balance of costimulatory and coinhibitory signals, and the availability and prior priming of peripheral T cells. Therapeutically, this suggests a new way to think about microglia in AD: not simply as phagocytes or inflammatory cells, but as genetically regulated mediators of antigen presentation whose interaction with adaptive immunity may be steered to preserve immune control while limiting chronic neuroinflammation.

References

1. Keren-Shaul, H. *et al.* A Unique Microglia Type Associated with Restricting Development of Alzheimer's Disease. *Cell* **169**, 1276-1290.e17 (2017).
2. Krasemann, S. *et al.* The TREM2-APOE Pathway Drives the Transcriptional Phenotype of Dysfunctional Microglia in Neurodegenerative Diseases. *Immunity* **47**, 566-581.e9 (2017).
3. Sala Frigerio, C. *et al.* The Major Risk Factors for Alzheimer's Disease: Age, Sex, and Genes Modulate the Microglia Response to Aβ Plaques. *Cell Reports* **27**, 1293-1306.e6 (2019).
4. Chen, W.-T. *et al.* Spatial Transcriptomics and In Situ Sequencing to Study Alzheimer's Disease. *Cell* **182**, 976-991.e19 (2020).
5. Mancuso, R. *et al.* Xenografted human microglia display diverse transcriptomic states in response to Alzheimer's disease-related amyloid-β pathology. *Nat Neurosci* 1–15 (2024).
6. Podleśny-Drabiniok, A., Marcora, E. & Goate, A. M. Microglial Phagocytosis: A Disease-Associated Process Emerging from Alzheimer's Disease Genetics. *Trends in Neurosciences* **43**, 965–979 (2020).
7. Mattiace, L. A., Davies, P. & Dickson, D. W. Detection of HLA-DR on microglia in the human brain is a function of both clinical and technical factors. *Am J Pathol* **136**, 1101–1114 (1990).
8. Styren, S. D., Civin, W. H. & Rogers, J. Molecular, cellular, and pathologic characterization of HLA-DR immunoreactivity in normal elderly and Alzheimer's disease brain. *Experimental Neurology* **110**, 93–104 (1990).
9. Perlmutter, L. S., Scott, S. A., Barrón, E. & Chui, H. C. MHC class II-positive microglia in human brain: Association with alzheimer lesions. *Journal of Neuroscience Research* **33**, 549–558 (1992).
10. Gehrmann, J., Banati, R. B. & Kreutzberg, G. W. Microglia in the immune surveillance of the brain: Human microglia constitutively express HLA-DR molecules. *Journal of Neuroimmunology* **48**, 189–198 (1993).
11. Parachikova, A. *et al.* Inflammatory changes parallel the early stages of Alzheimer disease. *Neurobiology of Aging* **28**, 1821–1833 (2007).

12. Hopperton, K. E., Mohammad, D., Trépanier, M. O., Giuliano, V. & Bazinet, R. P. Markers of microglia in post-mortem brain samples from patients with Alzheimer's disease: a systematic review. *Mol Psychiatry* **23**, 177–198 (2018).
13. Sun, N. *et al.* Human microglial state dynamics in Alzheimer's disease progression. *Cell* **186**, 4386-4403.e29 (2023).
14. Olah, M. *et al.* Single cell RNA sequencing of human microglia uncovers a subset associated with Alzheimer's disease. *Nature Communications* **11**, 6129 (2020).
15. Sayed, F. A. *et al.* AD-linked R47H-TREM2 mutation induces disease-enhancing microglial states via AKT hyperactivation. *Science Translational Medicine* **13**, eabe3947 (2021).
16. Gerrits, E. *et al.* Distinct amyloid-β and tau-associated microglia profiles in Alzheimer's disease. *Acta Neuropathol* **141**, 681–696 (2021).
17. Mancuso, R. *et al.* Stem-cell-derived human microglia transplanted in mouse brain to study human disease. *Nature Neuroscience* **22**, 2111–2116 (2019).
18. Hasselmann, J. *et al.* Development of a Chimeric Model to Study and Manipulate Human Microglia In Vivo. *Neuron* **103**, 1016-1033.e10 (2019).
19. McQuade, A. *et al.* Gene expression and functional deficits underlie TREM2-knockout microglia responses in human models of Alzheimer's disease. *Nature Communications* **11**, 5370 (2020).
20. Claes, C. *et al.* The P522R protective variant of PLCG2 promotes the expression of antigen presentation genes by human microglia in an Alzheimer's disease mouse model. *Alzheimer's & Dementia* **18**, 1765–1778 (2022).
21. Roche, P. A. & Cresswell, P. Antigen Processing and Presentation Mechanisms in Myeloid Cells. *Microbiology Spectrum* **4**, 10.1128/microbiolspec.mchd-0008–2015 (2016).
22. Sutter, P. A. & Crocker, S. J. Glia as antigen-presenting cells in the central nervous system. *Current Opinion in Neurobiology* **77**, 102646 (2022).
23. Chen, L. & Flies, D. B. Molecular mechanisms of T cell co-stimulation and co-inhibition. *Nat Rev Immunol* **13**, 227–242 (2013).

24. Kim, M. W. *et al.* Endogenous self-peptides guard immune privilege of the central nervous system. *Nature* **637**, 176–183 (2025).
25. Chen, D. *et al.* CTLA-4 blockade induces a microglia-Th1 cell partnership that stimulates microglia phagocytosis and anti-tumor function in glioblastoma. *Immunity* **56**, 2086-2104.e8 (2023).
26. Chen, X. *et al.* Microglia-mediated T cell infiltration drives neurodegeneration in tauopathy. *Nature* 1–10 (2023) doi:10.1038/s41586-023-05788-0.
27. Merlini, M., Kirabali, T., Kulic, L., Nitsch, R. M. & Ferretti, M. T. Extravascular CD3+ T Cells in Brains of Alzheimer Disease Patients Correlate with Tau but Not with Amyloid Pathology: An Immunohistochemical Study. *Neurodegener Dis* **18**, 49–56 (2018).
28. Togo, T. *et al.* Occurrence of T cells in the brain of Alzheimer's disease and other neurological diseases. *Journal of Neuroimmunology* **124**, 83–92 (2002).
29. Gate, D. *et al.* Clonally expanded CD8 T cells patrol the cerebrospinal fluid in Alzheimer's disease. *Nature* **577**, 399–404 (2020).
30. Monsonego, A. *et al.* Increased T cell reactivity to amyloid β protein in older humans and patients with Alzheimer disease. *J. Clin. Invest.* **112**, 415–422 (2003).
31. Rickenbach, C. *et al.* Altered T-cell reactivity in the early stages of Alzheimer's disease. *Brain* awaf167 (2025) doi:10.1093/brain/awaf167.
32. Dhanwani, R. *et al.* T Cell Responses to Neural Autoantigens Are Similar in Alzheimer's Disease Patients and Age-Matched Healthy Controls. *Front. Neurosci.* **14**, (2020).
33. Mittal, K. *et al.* CD4 T Cells Induce A Subset of MHCII-Expressing Microglia that Attenuates Alzheimer Pathology. *iScience* **16**, 298–311 (2019).
34. Le Guen, Y. *et al.* Multiancestry analysis of the HLA locus in Alzheimer's and Parkinson's diseases uncovers a shared adaptive immune response mediated by HLA-DRB1*04 subtypes. *Proceedings of the National Academy of Sciences* **120**, e2302720120 (2023).

35. Das, P., Chapoval, S., Howard, V., David, C. S. & Golde, T. E. Immune responses against Aβ1–42 in HLA class II transgenic mice: implications for Aβ1–42 immune-mediated therapies. *Neurobiology of Aging* **24**, 969–976 (2003).
36. Zota, V. *et al.* HLA-DR Alleles in Amyloid β-Peptide Autoimmunity: A Highly Immunogenic Role for the DRB1*1501 Allele1. *The Journal of Immunology* **183**, 3522–3530 (2009).
37. Sierksma, A. *et al.* Polygenic risk for Alzheimer's disease shapes microglial inflammatory and antigen-presentation programs in vivo. Preprint at https://doi.org/10.21203/rs.3.rs-7794221/v1 (2025).
38. Bellenguez, C. *et al.* New insights into the genetic etiology of Alzheimer's disease and related dementias. *Nat Genet* 1–25 (2022) doi:10.1038/s41588-022-01024-z.
39. Nott, A. *et al.* Brain cell type–specific enhancer–promoter interactome maps and disease-risk association. *Science* **366**, 1134–1139 (2019).
40. Kozlova, A. *et al.* PICALM Alzheimer's risk allele causes aberrant lipid droplets in microglia. *Nature* 1–9 (2025) doi:10.1038/s41586-025-09486-x.
41. Miller, S. E. *et al.* CALM Regulates Clathrin-Coated Vesicle Size and Maturation by Directly Sensing and Driving Membrane Curvature. *Developmental Cell* **33**, 163–175 (2015).
42. Tian, Y., Chang, J. C., Fan, E. Y., Flajolet, M. & Greengard, P. Adaptor complex AP2/PICALM, through interaction with LC3, targets Alzheimer's APP-CTF for terminal degradation via autophagy. *Proceedings of the National Academy of Sciences* **110**, 17071–17076 (2013).
43. Sjöstedt, E. *et al.* An atlas of the protein-coding genes in the human, pig, and mouse brain. *Science* **367**, eaay5947 (2020).
44. Colbert, J. D., Cruz, F. M. & Rock, K. L. Cross-presentation of exogenous antigens on MHC I molecules. *Current Opinion in Immunology* **64**, 1–8 (2020).
45. Heath, W. R. & Carbone, F. R. Cross-Presentation, Dendritic Cells, Tolerance and Immunity. *Annual Review of Immunology* **19**, 47–64 (2001).

46. Cruz, F. M., Colbert, J. D., Merino, E., Kriegsman, B. A. & Rock, K. L. The Biology and Underlying Mechanisms of Cross-Presentation of Exogenous Antigens on MHC-I Molecules. *Annu. Rev. Immunol.* **35**, 149–176 (2017).
47. Fattorelli, N. *et al.* Stem-cell-derived human microglia transplanted into mouse brain to study human disease. *Nature Protocols* 1–22 (2021).
48. Roche, P. A. & Furuta, K. The ins and outs of MHC class II-mediated antigen processing and presentation. *Nat Rev Immunol* **15**, 203–216 (2015).
49. Serneels, L. *et al.* Modeling the β-secretase cleavage site and humanizing amyloid-beta precursor protein in rat and mouse to study Alzheimer's disease. *Molecular Neurodegeneration* **15**, 60 (2020).
50. Saito, T. *et al.* Single App knock-in mouse models of Alzheimer's disease. *Nature Neuroscience* **17**, 661–663 (2014).
51. Smith, X. *et al.* The Chemokine CXCL12 Generates Costimulatory Signals in T Cells to Enhance Phosphorylation and Clustering of the Adaptor Protein SLP-76. *Science Signaling* **6**, ra65–ra65 (2013).
52. McGeer, P. L., Itagaki, S., Tago, H. & McGeer, E. G. Reactive microglia in patients with senile dementia of the Alzheimer type are positive for the histocompatibility glycoprotein HLA-DR. *Neurosci Lett* **79**, 195–200 (1987).
53. Tooyama, I., Kimura, H., Akiyama, H. & McGeer, P. L. Reactive microglia express class I and class II major histocompatibility complex antigens in Alzheimer's disease. *Brain Res* **523**, 273–280 (1990).
54. Kalaria, R. N. Microglia and Alzheimer's disease. *Curr Opin Hematol* **6**, 15–24 (1999).
55. Heyder, T. *et al.* Approach for Identifying Human Leukocyte Antigen (HLA)-DR Bound Peptides from Scarce Clinical Samples*. *Molecular & Cellular Proteomics* **15**, 3017–3029 (2016).
56. Wang, J. *et al.* HLA-DR15 Molecules Jointly Shape an Autoreactive T Cell Repertoire in Multiple Sclerosis. *Cell* **183**, 1264-1281.e20 (2020).

57. Willems, P. *et al.* Maximizing Immunopeptidomics-Based Bacterial Epitope Discovery by Multiple Search Engines and Rescoring. *J. Proteome Res.* **24**, 2141–2151 (2025).
58. Gul, A. *et al.* A platform for high-throughput and ultrasensitive immunopeptidomics. 2026.02.23.707388 Preprint at https://doi.org/10.64898/2026.02.23.707388 (2026).
59. Bathini, M. *et al.* MHC1-TIP enables single-tube multimodal immunopeptidome profiling and uncovers intratumoral heterogeneity in antigen presentation. *Commun Biol* **9**, 296 (2026).
60. Phulphagar, K. M. *et al.* Sensitive, High-Throughput HLA-I and HLA-II Immunopeptidomics Using Parallel Accumulation-Serial Fragmentation Mass Spectrometry. *Molecular & Cellular Proteomics* **22**, (2023).
61. Klaisner, S. *et al.* Large-scale HLA immunopeptidome and interactome profiling in microglia. 2025.04.23.650327 Preprint at https://doi.org/10.1101/2025.04.23.650327 (2025).
62. Boskovic, P. *et al.* Engineering chimeric antigen receptor CD4 T cells for Alzheimer's disease. *Proceedings of the National Academy of Sciences* **123**, e2530977123 (2026).
63. Cai, Y. *et al.* Immunopeptidomics-guided discovery and characterization of neoantigens for personalized cancer immunotherapy. *Science Advances* **11**, eadv6445 (2025).
64. Schaettler, M. O. *et al.* Characterization of the Genomic and Immunologic Diversity of Malignant Brain Tumors through Multisector Analysis. *Cancer Discov* **12**, 154–171 (2022).
65. Sirkis, D. W. *et al.* Expansion of highly interferon-responsive T cells in early-onset Alzheimer's disease. *Alzheimer's & Dementia* **20**, 5062–5070 (2024).
66. Hu, H. *et al.* CD8+ T cells are primed by cDC1 and exacerbate tau-mediated neurodegeneration. 2026.02.26.708260 Preprint at https://doi.org/10.64898/2026.02.26.708260 (2026).
67. Ayata, P. *et al.* Lymphoid gene expression supports neuroprotective microglia function. *Nature* **648**, 157–165 (2025).
68. Park, T. *et al.* Targeting glial PD-1/PD-L1 restores microglial homeostasis and attenuates neuronal hyperactivity in an Alzheimer's disease model. 2024.09.13.612389 Preprint at https://doi.org/10.1101/2024.09.13.612389 (2025).

69. Kimura, K. *et al.* Immune checkpoint TIM-3 regulates microglia and Alzheimer's disease. *Nature* **641**, 718–731 (2025).

70. Su, W. *et al.* CXCR6 orchestrates brain CD8+ T cell residency and limits mouse Alzheimer's disease pathology. *Nat Immunol* **24**, 1735–1747 (2023).

71. Filipello, F. *et al.* Defects in lysosomal function and lipid metabolism in human microglia harboring a TREM2 loss of function mutation. *Acta Neuropathol* **145**, 749–772 (2023).

72. Voytik, E. *et al.* AlphaMap: an open-source Python package for the visual annotation of proteomics data with sequence-specific knowledge. *Bioinformatics* **38**, 849–852 (2022).

73. Sirvent, D. Á. *et al.* Cognitively healthy centenarians are characterized by lower frequencies of six disease-associated HLA alleles. 2025.03.30.25324899 Preprint at https://doi.org/10.1101/2025.03.30.25324899 (2025).

74. Zheng, X. *et al.* HIBAG—HLA genotype imputation with attribute bagging. *Pharmacogenomics J* **14**, 192–200 (2014).

75. Demichev, V., Messner, C. B., Vernardis, S. I., Lilley, K. S. & Ralser, M. DIA-NN: neural networks and interference correction enable deep proteome coverage in high throughput. *Nat Methods* **17**, 41–44 (2020).

76. Ammar, C. *et al.* Tree-based quantification infers proteoform regulation in bottom-up proteomics data. 2025.03.06.641844 Preprint at https://doi.org/10.1101/2025.03.06.641844 (2025).

77. Kong, A. T., Leprevost, F. V., Avtonomov, D. M., Mellacheruvu, D. & Nesvizhskii, A. I. MSFragger: ultrafast and comprehensive peptide identification in mass spectrometry-based proteomics. *Nat Methods* **14**, 513–520 (2017).

78. Eng, J. K., Jahan, T. A. & Hoopmann, M. R. Comet: an open-source MS/MS sequence database search tool. *Proteomics* **13**, 22–24 (2013).

79. Lazear, M. R. Sage: An Open-Source Tool for Fast Proteomics Searching and Quantification at Scale. *J Proteome Res* **22**, 3652–3659 (2023).

80. Zhang, J. *et al.* PEAKS DB: de novo sequencing assisted database search for sensitive and accurate peptide identification. *Mol Cell Proteomics* **11**, M111.010587 (2012).
81. Declercq, A. *et al.* TIMS2Rescore: A Data Dependent Acquisition-Parallel Accumulation and Serial Fragmentation-Optimized Data-Driven Rescoring Pipeline Based on MS2Rescore. *J Proteome Res* **24**, 1067–1076 (2025).
82. Reynisson, B., Alvarez, B., Paul, S., Peters, B. & Nielsen, M. NetMHCpan-4.1 and NetMHCIIpan-4.0: improved predictions of MHC antigen presentation by concurrent motif deconvolution and integration of MS MHC eluted ligand data. *Nucleic Acids Res* **48**, W449–W454 (2020).
83. Nilsson, J. B. *et al.* Accurate prediction of HLA class II antigen presentation across all loci using tailored data acquisition and refined machine learning. *Sci Adv* **9**, eadj6367 (2023).
84. Andreatta, M., Alvarez, B. & Nielsen, M. GibbsCluster: unsupervised clustering and alignment of peptide sequences. *Nucleic Acids Res* **45**, W458–W463 (2017).
85. Kolberg, L. *et al.* g:Profiler-interoperable web service for functional enrichment analysis and gene identifier mapping (2023 update). *Nucleic Acids Res* **51**, W207–W212 (2023).
86. Hunter, J. D. Matplotlib: A 2D Graphics Environment. *Computing in Science & Engineering* **9**, 90–95 (2007).
87. Waskom, M. L. seaborn: statistical data visualization. *Journal of Open Source Software* **6**, 3021 (2021).
88. Tareen, A. & Kinney, J. B. Logomaker: beautiful sequence logos in Python. *Bioinformatics* **36**, 2272–2274 (2020).
89. Gayoso, A. *et al.* Joint probabilistic modeling of single-cell multi-omic data with totalVI. *Nat Methods* **18**, 272–282 (2021).
90. De Rop, F. V. *et al.* Hydrop enables droplet-based single-cell ATAC-seq and single-cell RNA-seq using dissolvable hydrogel beads. *eLife* **11**, e73971 (2022).
91. Butler, A., Hoffman, P., Smibert, P., Papalexi, E. & Satija, R. Integrating single-cell transcriptomic data across different conditions, technologies, and species. *Nat Biotechnol* **36**, 411–420 (2018).

92. Stuart, T. *et al.* Comprehensive Integration of Single-Cell Data. *Cell* **177**, 1888-1902.e21 (2019).
93. Hafemeister, C. & Satija, R. Normalization and variance stabilization of single-cell RNA-seq data using regularized negative binomial regression. *Genome Biology* **20**, 296 (2019).
94. Korsunsky, I. *et al.* Fast, sensitive and accurate integration of single-cell data with Harmony. *Nat Methods* **16**, 1289–1296 (2019).
95. Lau, S.-F., Wu, W., Seo, H., Fu, A. K. Y. & Ip, N. Y. Quantitative in vivo assessment of amyloid-beta phagocytic capacity in an Alzheimer's disease mouse model. *STAR Protocols* **2**, 100265 (2021).

Acknowledgements

We warmly thank Veronique Hendrickx and Amber Claes for animal husbandry and genotyping; Leen Wolfs for single cell library preparations; Suresh Poovathingal, and Marta Wojno from the Single Cell Microfluidics & Analytics and Bioinformatics unit (VIB-CNL) for help with library preparations and sequencing; Niels Vandamme from the VIB Single Cell Core for CITEseq library preparation and sequencing for scRNAseq and CITEseq; Pedro Magalhães (VIB Metabolomics Core Leuven) for proteomics advice; Pengfei Hou and Pranav Preman for technical assistance; and members of the De Strooper lab for paper discussions. We would like to express our appreciation to the donors of the Netherlands Brain Bank, and their family members.

Funding: this project received funding from:

Stichting Onderzoek Alzheimer, SAO-FRA 20220023 (SCB & BDS)

Alzheimer's Association USA, E2A-23-1149216 (BDS)

European Research Council (ERC), ERC-834682 "CELLPHASE_AD" (BDS)

KU Leuven & Flemish Government, Methusalem METH/21/05 (BDS)

Flanders Institute for Biotechnology (VIB vzw) (BDS, MM, EP, FI)

Bax-Vanluffelen Chair for Alzheimer's Disease (BDS)

Author contributions

Conceptualization: BDS, ASi, SCB

Investigation and methodology: SCB, ASi, EP, LVM, PW, DM, PB, NT, ASn, RL, DT'S, AFL, BG, HDB, AG, DAS

Writing – original draft: SCB, BDS

Writing – review and editing: all authors

Resources: NM, DW, IH, NBB

Supervision: BDS, ASi, MF, FI, VM, EP, MM, HH

Funding acquisition: BDS, SCB

Competing interests:

B.D.S. has been a consultant for Eli Lilly, Biogen, Janssen Pharmaceutica, Eisai, AbbVie and other companies and is now consultant to Muna Therapeutics. B.D.S is a scientific founder of Augustine Therapeutics and a scientific founder and stockholder of Muna Therapeutics. B.D.S. is also a member of the scientific advisory board of Cell. M.F. is a consultant to Muna Therapeutics.

Data and materials availability:

Requests for further information and resources should be directed to and will be fulfilled by the lead contact, Bart De Strooper (b.strooper@ukdri.ac.uk). The raw mass spectrometry data for the immunopeptidomics studies have been deposited to the ProteomeXchange Consortium via the PRIDE partner repository with the dataset identifier PXD077580 (reviewer login: reviewer_pxd077580@ebi.ac.uk and password: uUG2P7VKKEyn). Raw proteomic data from xenografted microglia studies will be deposited in the PRIDE repository with dataset

identifier [INSERT] Sequencing data will be deposited in the EGA database under accession number [INSERT] and made accessible behind a data access committee.

Figures and Figure Legends

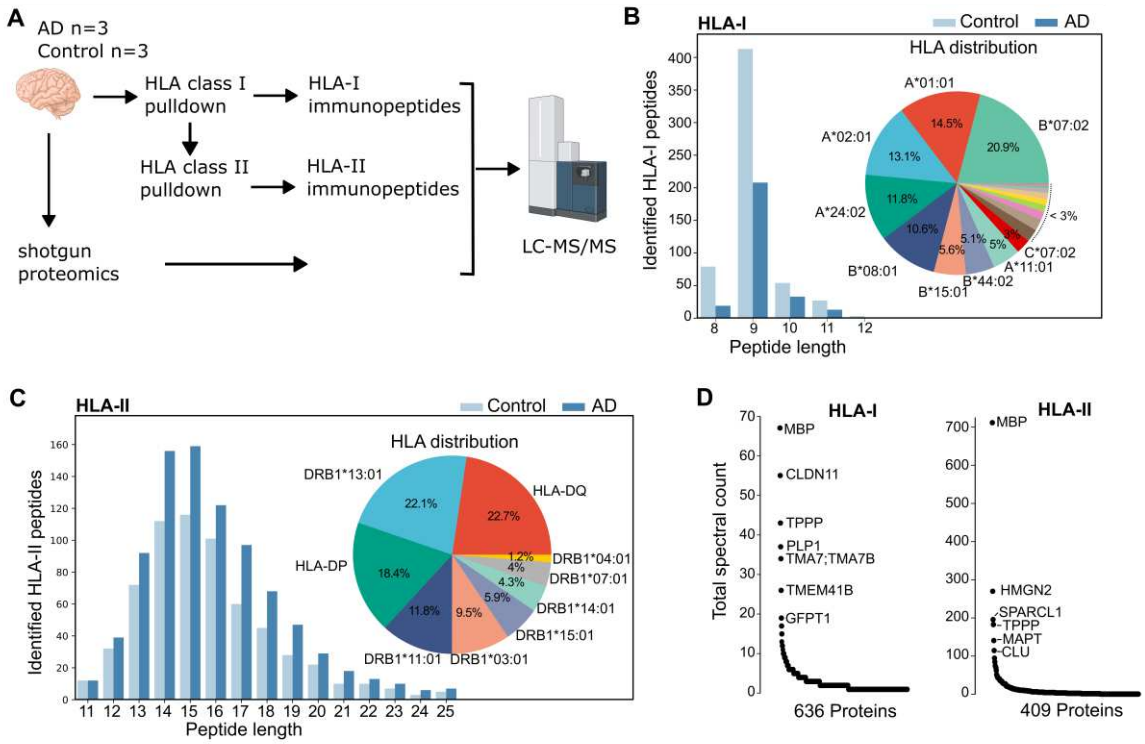


Figure 1. HLA-I and HLA-II peptide repertoires are detected in human Alzheimer brain tissue

(A) Using superior frontal gyrus of AD cases (n=3) and controls (n=3), shotgun proteomics and sequential pulldowns for HLA class I and HLA class II complexes and immunopeptide purification performed, followed by mass spectrometry. (B) Peptide length and HLA distribution of identified HLA-I binding peptides (%Rank < 2 NetMHCpan-4.1) in AD and control samples. For the distribution, the HLA allele with the strongest binding prediction was used. (C) Peptide length and HLA distribution of identified HLA-II binding peptides (% Rank < 5 NetMHCIIpan-4.3) in AD and control samples. (D) Relative protein levels represented as total spectral counts for all corresponding HLA-I peptides (left) and HLA-II peptides (right) across the whole dataset (n=6 samples), x axis is ordered by frequency.

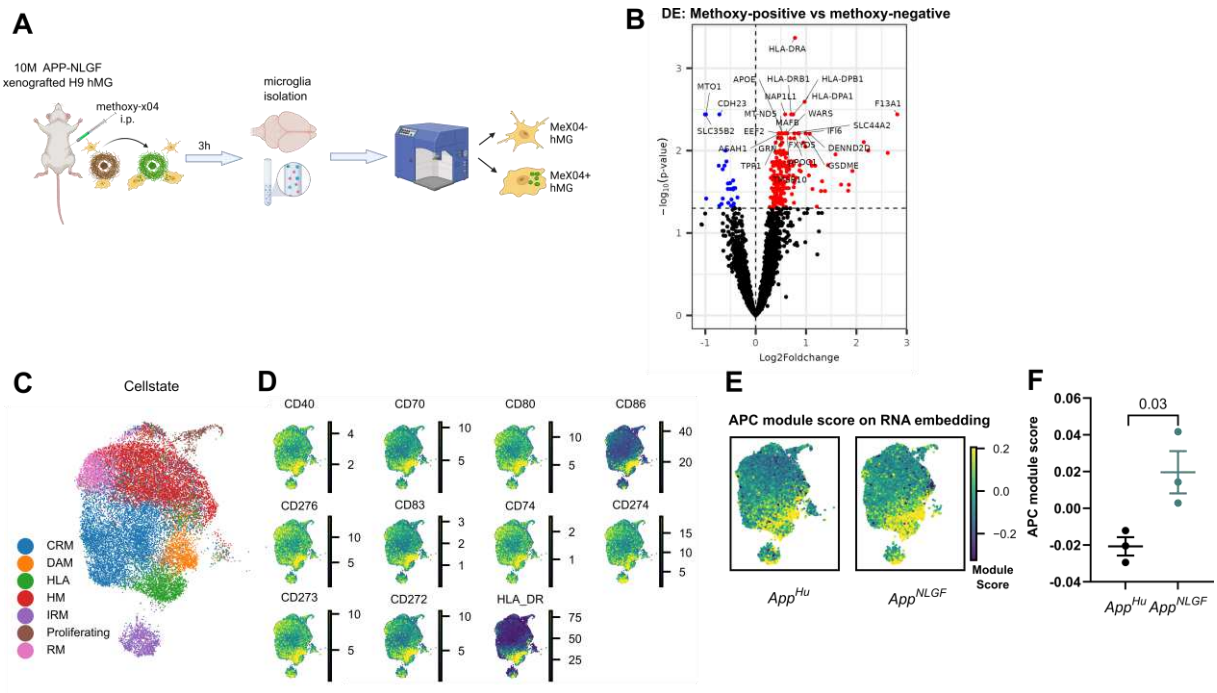


Figure 2: Human xenografted microglia upregulate an antigen presenting cell module in response to amyloid exposure

(A) Experimental design of methoxy-X04 *in vivo* phagocytosis experiments on human xenografted microglia from *App*^{NLGF}. (B) Volcano plot of log2(FC) differentially expressed genes between Methoxy-X04 positive and Methoxy-X04 negative microglia from n = 8 *App*^{NLGF} mice. DEGs upregulated in methoxy-X04-positive microglia are shown in red, those downregulated are shown in blue (Benjamini–Hochberg–adjusted $P < 0.05$). (C-F) CITEseq analysis of human xenografted microglia from *App*^{NLGF} (n=3 mice) and *App*^{Hu} mice (n=3 mice). (C) Integrated RNA UMAP demonstrating annotation of microglial states as previously defined[5]. (D) Projection of protein measurements onto the RNA UMAP showing the abundance of individual antigen presenting cell module proteins. Colour scale bar for each plot is relative expression. (E) APC score projected onto the RNA UMAP for *App*^{Hu} and *App*^{NLGF}, with yellow indicating cells with high APC module score. (F) Quantification of APC module in *App*^{Hu} and *App*^{NLGF} conditions (two-side unpaired Student's t-test, t=3.208, df=4, P=0.0326), graph shows mean±SEM with points presenting individual mice.

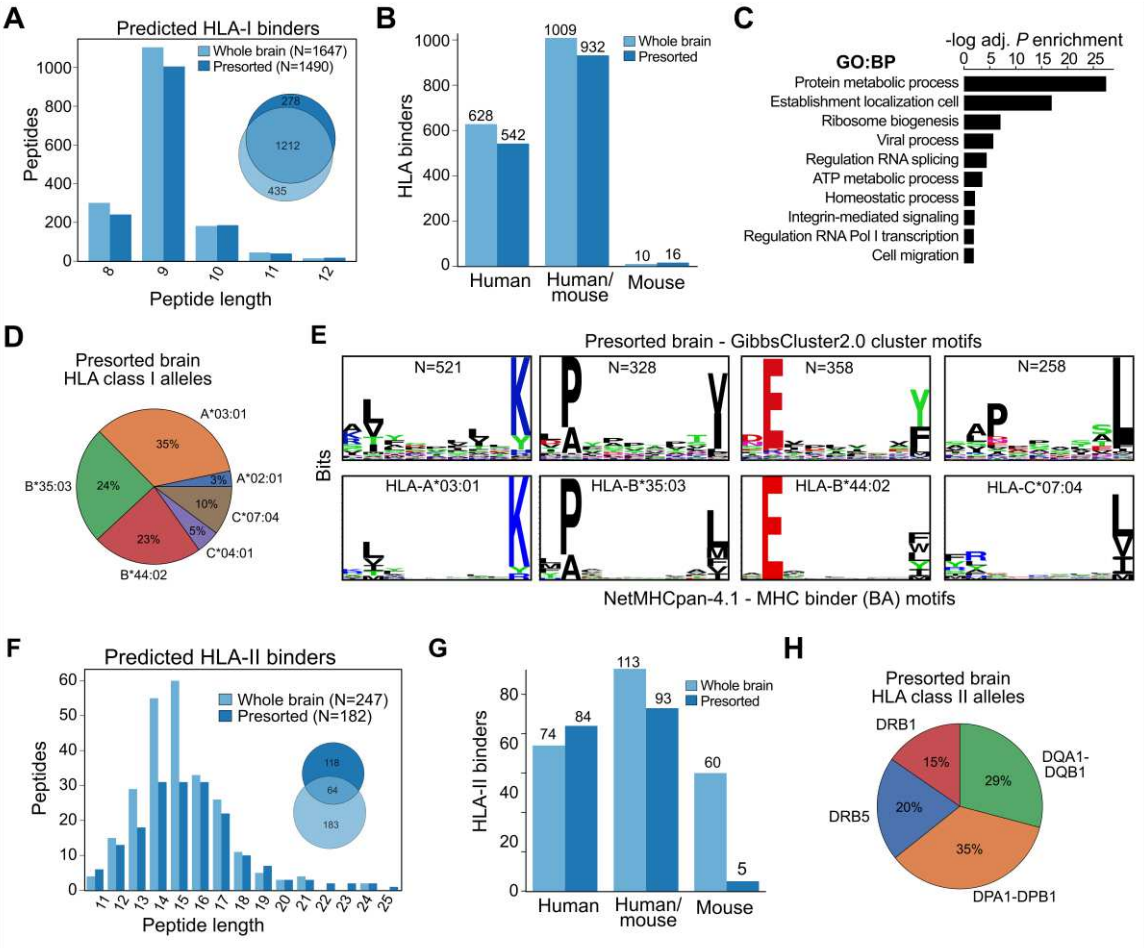


Figure 3: Presentation of immunopeptides bound to HLA complexes by human xenografted microglia in the context of Aβ pathology

(A-E) HLA-I immunopeptidomics of human xenografted microglia from *App*^{NLGF} mice, isolated either from whole brain (light blue, n=1) or after pre-sorting microglia (dark blue, n=1). (A) Length distribution of identified peptides predicted to bind human HLA class I (%Rank < 2 NetMHCpan-4.1). (B) Number of HLA-I binding peptides assigned by species. Human/mouse indicates peptide sequences shared between human and mouse proteins. (C) The top ten enriched gene ontology biological process (GO:BP) terms after functional enrichment analysis by g:Profiler of source proteins from peptides shown in B). (D) Predicted HLA-I binding distribution of immunopeptides using NetMHCpan-4.1. For each peptide, the HLA allele with the best %Rank score was plotted. (E) Cluster peptide motifs identified by GibbsCluster2.0 from all identified peptides in the presorted brain samples (top) compared with theoretical NetMHCpan-4.1 binding affinity (BA) motifs (bottom). F-H) HLA-II immunopeptidomics of human xenografted microglia from *App*^{NLGF} mice, isolated either from whole brain (light blue) or after pre-sorting for microglia (dark blue). (F) Length distribution of identified HLA-II binding peptides (%Rank < 5 NetMHCIIpan-4.3). (G) Number of HLA-II binding peptides assigned by species. Human/mouse indicates peptide sequences shared between the human and mouse proteins. (H) Predicted HLA class II binding distribution of immunopeptides using NetMHCIIpan-4.3. For each peptide, the HLA allele with the best %Rank score was plotted.

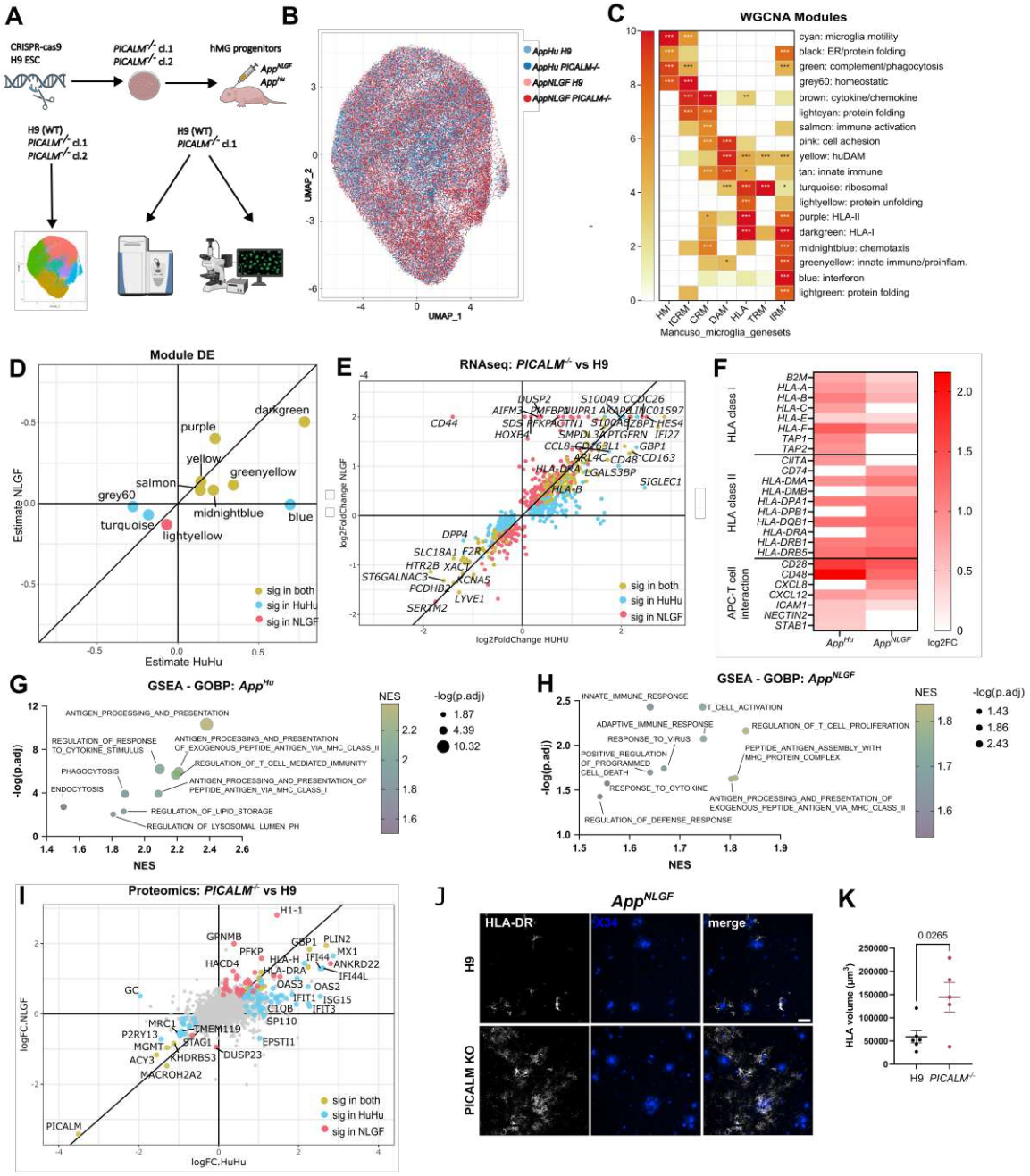


Figure 4: Loss of the AD risk gene PICALM amplifies HLA responses in human microglia exposed to Aβ plaque pathology

(A) Experimental design. (B-H) scRNAseq analysis on microglia isolated from *App*^{NLGF} grafted with H9 (n=12 mice: batch 1 n=6, batch 2 n=6) and *PICALM*$^{-/-}$ (n=12 mice: batch 1 cl.1 n=6, batch 2 cl.2 n=6) and *App*^{hu} grafted with H9 (n=11 mice: batch 1 n=5, batch 2 n=6) and *PICALM*$^{-/-}$ (n=11 mice: batch 1 cl.1 n=5, batch 2 cl.2 n=6). (B) Integrated UMAP from both batches. (C) WGCNA module analysis plotted against microglia cell states[5]. (D) Quadrant plot of differential WGCNA module eigen-gene expression between *App*^{NLGF} and *App*^{hu} comparing *PICALM*$^{-/-}$ with H9 microglia. Modules in yellow are altered in both *App*^{NLGF} and *App*^{hu}, whereas modules in blue are significant in *App*^{hu} only (Benjamini–Hochberg–adjusted $P < 0.05$). (E) Quadrant plot of differential gene expression pseudobulked from scRNAseq data by hMG genotype and mouse strain, (Benjamini–Hochberg–adjusted $P < 0.05$). (F) Heatmap of log2(FC) expression of HLA and APC-associated genes in *PICALM*$^{-/-}$ vs H9 by strain (*P*adj. <0.05). (G) GSEA

analysis for *PICALM*$^{-/-}$ vs H9 *App*^{hu}, showing the top enriched GO biological pathways by NES (normalized enrichment score) and -log(p. adj). (H) GSEA analysis for *PICALM*$^{-/-}$ vs H9 *App*^{NLGF}, showing the top enriched GO biological pathways by NES and -log(p.adj). (I) Bulk proteomics analysis of *PICALM*$^{-/-}$ cl.1 vs H9 microglia (*App*^{NLGF} n = 6 mice/genotype, *App*^{hu} n=5 mice/genotype) shown as a quadrant plot comparing the differential protein expression in *App*^{hu} (x-axis) vs *App*^{NLGF} mice (y-axis). Benjamini-Hochberg adjusted $P < 0.05$. (J) Representative immunostaining for HLA-DR in *App*^{NLGF} mice for H9 and *PICALM*$^{-/-}$ human microglia. (K) Quantification of the HLA-positive human microglia population in H9 (n = 6) and *PICALM*$^{-/-}$ (n=5) *App*^{NLGF} brains (two-tailed unpaired t test, t=2.650, df=9, *P*=0.0265). Scale bar 50µm.

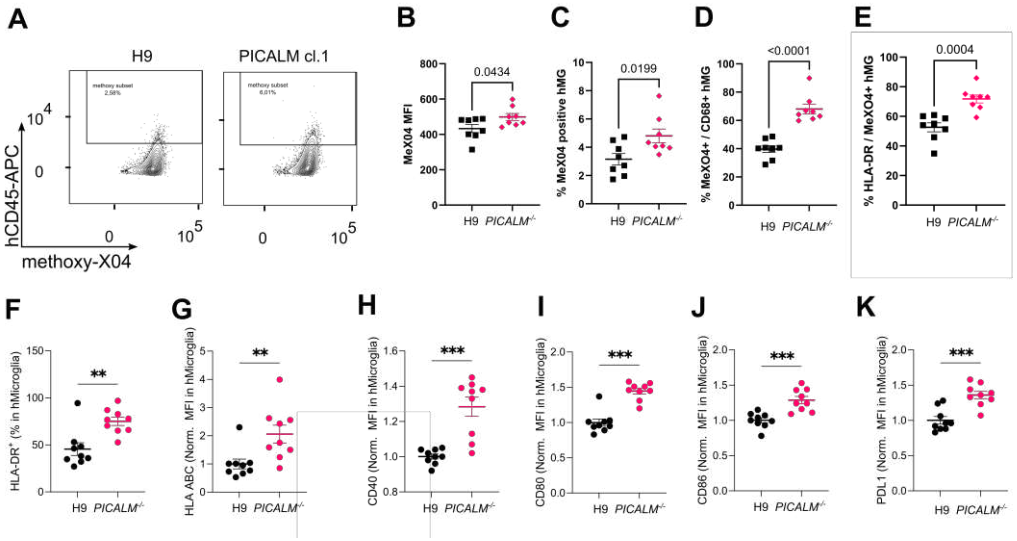
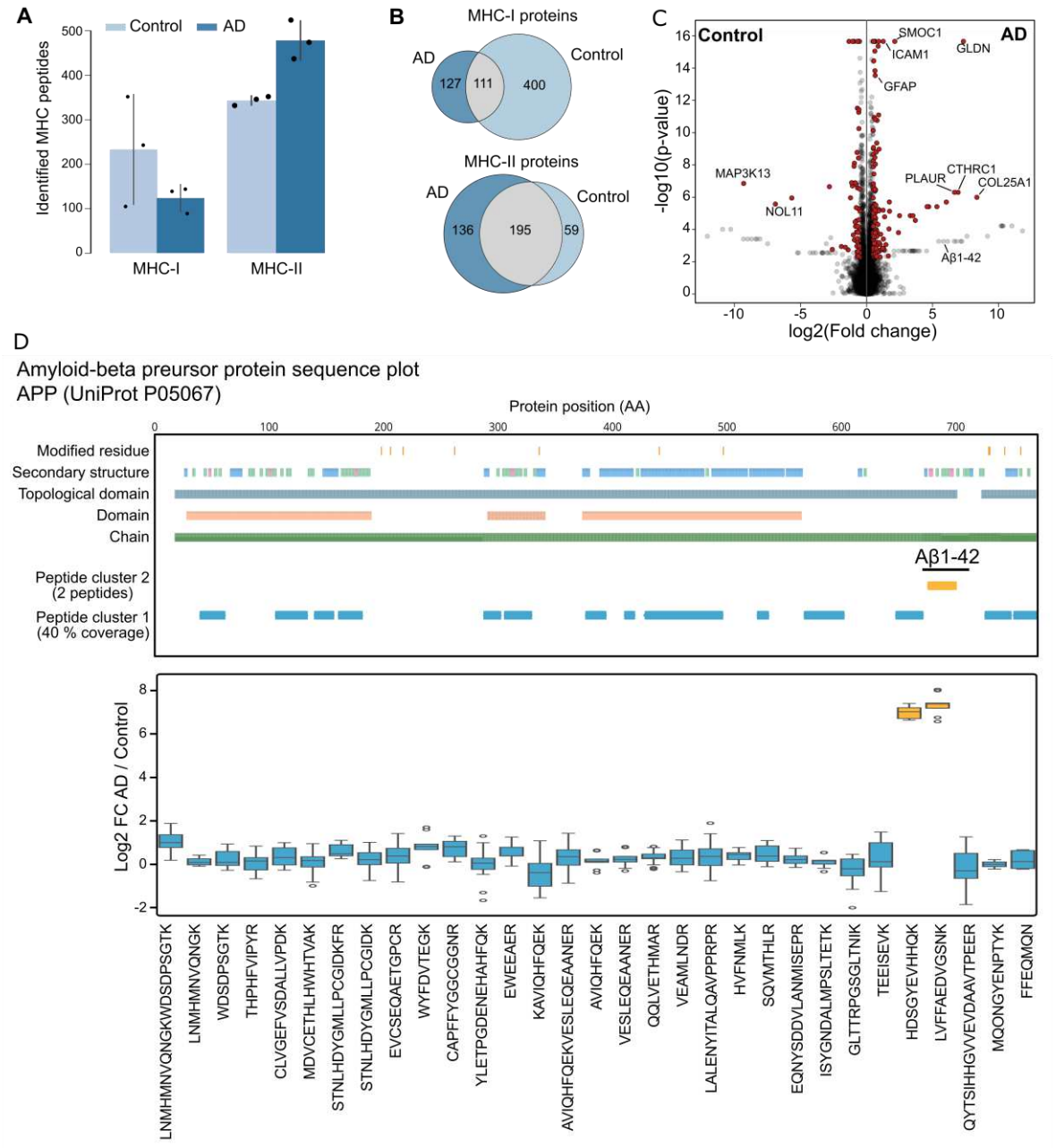


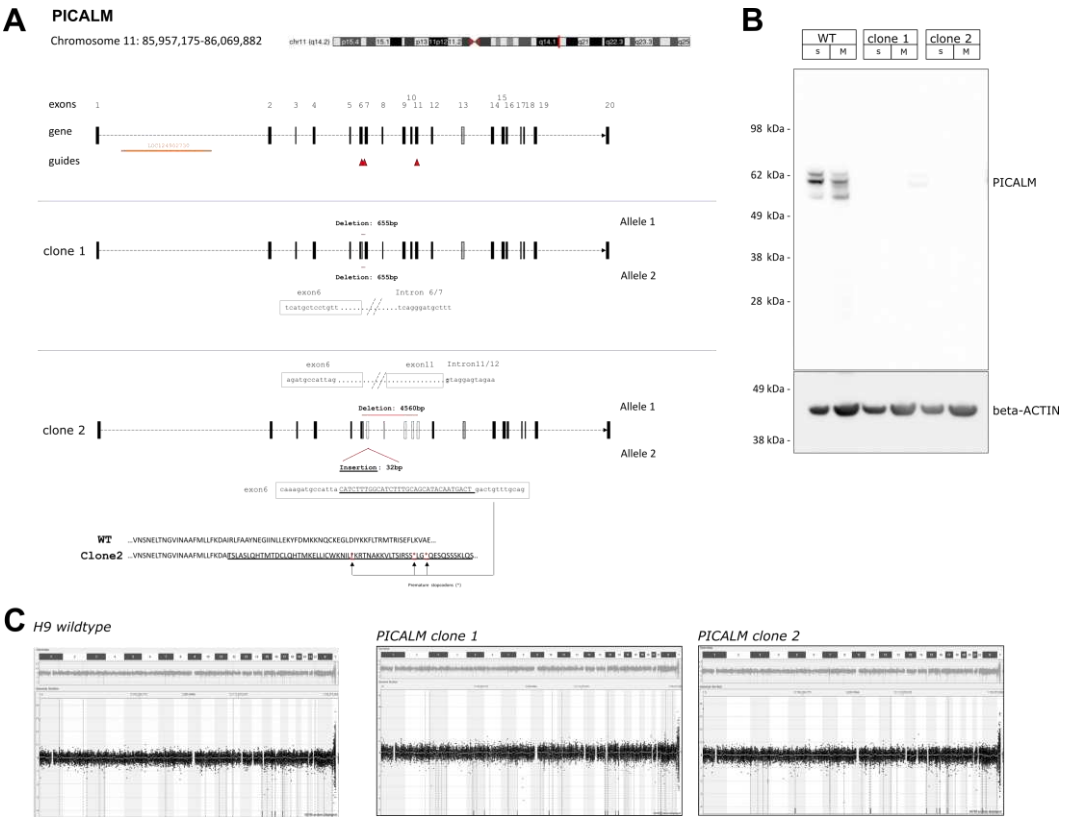
Figure 5. In response to amyloid pathology, *PICALM*$^{-/-}$ human microglia increase Aβ accumulation and upregulate APC markers

(A-E) FACS analysis of Methoxy-X04 incorporation into H9 (n=8 mice) and *PICALM*$^{-/-}$ microglia (n=8 mice) isolated from 10M *App*^{NLGF}, 3 hours after injection. (A) Representative FACS plots and gating strategy for detection of methoxy-X04 signal in human microglia. (B) Methoxy-X04 mean fluorescence intensity (MFI) methoxy-X04 positive cells in hCD45-positive microglia (two-tailed unpaired t test, t=2.2221, df=14, *P*=0.0434). (C) Percentage of methoxy-X04 positive cells in hCD45-positive microglia (two-tailed unpaired t test (t=2.627, df=14, *P*=0.0199). (D) Percentage methoxy-X04 positive CD68-high microglia cells (two-tailed unpaired t test (t=6.731, df=14, *P*<0.0001). (E) Percentage of human HLA-DR-positive cells within the methoxy-X04-positive subset (two-tailed unpaired t test (t=4.659, df=14, *P*=0.0004). (F-K) FACS analysis of APC markers in H9 and *PICALM*$^{-/-}$ microglia isolated from 6M *App*^{NLGF}, n=9/genotype. (F) Quantification of percentage of HLA-DR positive cells in human CD45+ population (two-tailed Mann-Whitney *U*=9, *P*=0.0040). (G) normalized HLA-ABC MFI (two-tailed Mann-Whitney *U*=9, *P*=0.0037). (H-K) Quantification of CD40 (two-tailed Mann-Whitney *U*=9, *P*=0.0004), CD80 (two-tailed Mann-Whitney *U*=2, *P*=0.0002), CD86 (two-tailed Mann-Whitney *U*=2.5, *P*=0.0002) and PDL1 (two-tailed Mann-Whitney *U*=4, *P*=0.0005) MFI (normalized levels). B-K) All graphs are mean±SEM with points representing individual mice.



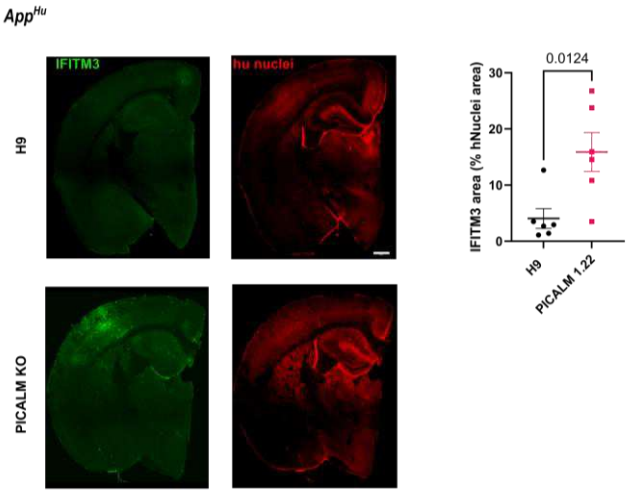
Supplemental Figure 1: Shotgun proteomics on human Alzheimer brain tissue

(A) Total number of unique identified peptides per sample for HLA-I and HLA-II immunopeptides, n=3 individuals/group. (B) Overlap of total number of unique proteins identified in HLA-I and HLA-II immunopeptidomes in AD and control groups. (C) Volcano plot of differentially expressed proteins in control vs AD samples from shotgun proteomics, n=3 individuals/group. DIA-NN search results were used for pairwise comparison (AD/control) in AlphaQuant. Significant proteins (red dots) represent statistically significant regulated proteins (FDR < 5%, absolute log2 fold change > 0.5) quantified by at least two peptide precursors. (D) Outlier peptides detected by AlphaQuant in the APP protein indicated a higher abundance of the Aβ1-42 sequence (proteoform FDR 1.106×10^{-9}). The protein sequence plot is made by AlphaMap[72] integrated in AlphaQuant.



Supplemental Figure 2: Generation and validation of *PICALM* KO clones

(A) Genomic map of *PICALM* illustrating the gene targeting strategy and indels generated in both clones after CRISPR/Cas9 gene editing. Guide targeting areas are indicated by red triangles. Indels (insertion or deletions) are indicated for both alleles in both clones. (B) Representative Western blot analysis of stem cells (s) and monocytes (m) showing the protein expression levels of PICALM and β-ACTIN following CRISPR-Cas9 gene editing. (C) Array CGH analysis of H9 and PICALM clones used in this study showed no chromosomal aberrations.



Supplemental Figure 3: Loss of PICALM upregulates IFITM3 under basal conditions

Representative IFITM3 staining, and quantification of IFITM3 area in *App*^{huhu} brain grafted with H9 and *PICALM*$^{-/-}$ (n=6 mice/genotype, two-tailed unpaired t test, t=3.042, df=10, *P*=0.0124). Scale bar 500µm, mean±SEM with points representing individual mice.

Methods

Human post-mortem brain samples

Human brain tissues were obtained from the Netherlands Brain Bank (NBB), Netherlands Institute for Neuroscience, Amsterdam. Written informed consent was given by the donors for brain autopsy and for the use of material and clinical data for research purposes, in compliance with national ethical guidelines. Brain tissue from 6 human autopsy cases were included in this study, as previously described[4]. We selected 3 individuals with clinically diagnosed as AD (amyloid stage C and Braak stage V-VI) and 3 non-demented controls (NDC) with no or very little pathology. All individuals were female and age-matched. Clinicopathological information of the donors including Ab deposition (stage A, B and C) and neurofibrillary tangles (stage I-VI) for these samples was previously reported[4]. Frozen tissue punches of superior frontal gyrus were stored at 80°C.

HLA genotyping

Genotyping of post-mortem donors from the Netherlands Brain Bank was performed using the Illumina Global Screening array version 3, as previously described (Mekkes et al., manuscript in preparation). Model-based HLA imputation was performed for human AD and control individuals as previously described[73]. HLA genotypes at two-fields allele resolution were imputed using the software HIBAG[74] and the prediction model specific to our population (of European ancestry) and genotyping platform. This model imputes alleles for all seven classical HLA class I and class II genes. Imputation was performed for all individuals retained after QC. After imputation, only genotypes with posterior probability >0.5 were kept, as recommended[74].

For HLA typing of the H9 ESC cell line, DNA extraction was performed on cell pellet with the PCI method. In short, cell pellets were lysed in cell lysis buffer (10mM Tris (pH 8), 100mM NaCl, 10mM EDTA (pH 8), 10% SDS) containing proteinase K (20 mg/ml) for 1h at 56°C with agitation (1400rpm). After adding phenol:chlorophorm:isoamyl alcohol (25:24:1, pH 7.8-8.2; Fluka Biochemika, cat# RA14615), vortexing for 1min and spinning at max speed for 5min, the aqueous phase was removed into a fresh tube. Additional retrieval was performed by adding elution buffer (10mM TrisHCl pH 8.5) to the cell lysate tube, vortexing and spinning at max speed, and removing the additional aqueous phase, which was merged with the initial aqueous phase. Next, equal volumes of chloroform:isoamyl alcohol (Sigma, cat# 0549-1PT) was added to the aqueous phase, samples were vortexed and spun at max speed for 5 min, after which the aqueous phase was again transferred to a clean tube. Ethanol precipitation was achieved by adding 0.75M NH4OAc (final concentration) and 20 µg of GlycoBlue (Invitrogen, cat# AM9516) to the sample, mixing and subsequently adding 2.5 volumes of 100% ethanol, mixing and incubating at -80°C for 30min. After a 20 min spin at full speed at 4°C, the supernatant was decanted, the samples were washed 2x in 80% ethanol and dried overnight at RT. Samples were resuspended in 60°C elution buffer and stored at -20°C until further handling. Genotyping of all samples to G-level resolution of the MHCII locus (exon 2 and 3 for HLA-A, -B, -C and exon 2 for HLA-DRB1345, -DQA1, -DQB1, DPA1, -DPB1) was performed using the HiSeq sequencing system (Illumina Inc., San Diego, USA). The IMGT/HLA allele database version 3.55.0 was used for results reporting.

Shotgun proteomics on human brain tissue

Sample preparation

5-10 mg human brain tissue was homogenized in 100 µL 5% SDS, 50 mM triethylammonium bicarbonate (TEAB) using a Pixul® multi-sample sonicator (Active Motif) for 2 times 10 minutes, N = 50, PRF1 kHz, burst rate 20 Hz. Following a 15-minute centrifugation step at

20,000g, protein concentrations were determined and normalized using BCA (#23225, Pierce). Reduction-alkylation was performed by adding 10 mM tris(2-carboxyethyl)phosphine (TCEP) and 40 mM chloroacetamine (CAA) to 100 µg protein extract in 50 µL lysis buffer, followed by a 10-minute incubation in the dark, using a thermomixer (95°C, 750 rpm). Samples were cooled to room temperature before acidification to pH < 1 using 1% phosphoric acid. Samples were mixed with 350 µL 100 mM TEAB 90% methanol (pH 7.55) before loading on S-trap™ mini spin columns (#C002-MINIX, Protifi), followed by 1-minute centrifugation at 4000g. Columns were washed three times with 400 µL 100 mM TEAB, 90% methanol (pH 7.55) before overnight incubation at 37°C with 1.5 µg trypsin in 125 µL 50 mM TEAB. The next day, digested peptides were eluted in 1) 80 µL 50 mM TEAB, 2) 0.1% formic acid and 3) 0.1% formic acid in 50% ACN, each time followed by 1-minute centrifugation at 4000g, and dried using a SpeedVac vacuum concentrator. The dried peptides were dissolved in 2% ACN, 0.1% TFA before loading on OMIX 100 µL C18 tips (#A57003100, Agilent), five times pre-washed with 80% ACN, 0.1% TFA and with 0.1% TFA. The loaded peptides were washed three times with 0.1% TFA before eluting in two times 100 µL 60% ACN, 0.1% TFA. The peptides were dried in an HPLC vial using a SpeedVac vacuum concentrator and stored at -20°C until LC-MS/MS injection.

LC-MS/MS

Peptides were re-dissolved in 20 µl loading solvent (0.1% trifluoroacetic acid in water/acetonitrile (ACN) (99.5:0.5, v/v)) of which 15 µl was injected for LC-MS/MS analysis on a Vanquish Neo system in-line connected to an Orbitrap Astral mass spectrometer (Thermo). Injection was performed in trap-and-Elute mode in combined control mode (maximum flow of 60 µl/min and maximum pressure of 800 bar) in Weak Wash solvent (WW, 0.1% trifluoroacetic acid in water) on a 5 mm trapping column (Pepmap, 300 µm internal diameter (I.D.), 5 µm beads, Thermo Scientific). The peptides were separated on an in-house produced column (75 µm x 100 mm), equipped with a laser pulled electrospray tip using a P-2000 Laser Based Micropipette Puller (Sutter Instruments), packed in-house with ReproSil Saphir 1.5 µm silica particles (Dr. Maisch). The column was kept at a constant temperature of 45°C. Peptides were eluted by a gradient starting at 0.5 % MS analytical solvent B (ASB, 0.1% FA in acetonitrile) reaching 26% ASB in 17 min, 44% ASB in 20 min, 56% ASB in 21 minutes followed by 4-minute wash at 56% ASB and column equilibration in Pressure Control mode (separation column: fast equilibration, maximum pressure of 1500 bar, equilibration factor=2; Trap column: fast wash and equilibration, wash factor=100, trap wash in pressure control with a max pressure of 800 bar) . The flow rate was set to 250 nl/min during the gradient run and at 300 nl/min in the equilibration step . The Orbitrap Astral was operated in Data independent mode at a full MS resolution of 240,000 with a full scan range of 380 − 980 *m/z*. The full MS AGC was set to 500%. Fragment ion scans were recorded at a resolution of 80,000 and maxIT of 3 ms. 300 windows of 2-Th scanning from 380-980 *m/z* were used to isolate and fragment ions using HCD with 25% NCE at an AGC target of 500% and a scan range of 150-2000 *m/z*. A loopcontrol of 0.6 s was applied.

Database search and differential proteomics analysis

DIA-NN (version 2.3.2)[75] was used to generate a spectral library for the human UniProtKB reference proteome (UP000005640, including splice forms, February 2026) appended with the human Aβ1-42 sequence and the built-in DIA-NN contaminant list. Tryptic peptide precursors of length 7-30, charge 1-4 and *m/z* 380-980 were predicted. One missed cleavage was allowed and cysteine carbamidomethylation was set as static modification, while methionine oxidation and N-terminal protein acetylation as variable modifications. Raw mass spectrometry data was searched against the spectral library on default settings using recommended orbitrap Astral settings of 10 ppm mass accuracy and 4 ppm MS1 precursor tolerance. The scan window radius was set to 6, and matching-between-runs was enabled. The resulting DIA-NN search

report was used as input for pairwise comparison (AD / control) in AlphaQuant[76] using default settings. A FDR < 5%, absolute log2 fold change > 0.5 and quantification by at least two peptide precursors was set as threshold to define significantly expressed proteins.

Immunopeptidomics

Generation of immunoaffinity resin for MHC Class I and II pull-down

W6/32 monoclonal pan-MHC class I and PdV5.2 monoclonal pan-MHC class II immunoaffinity resin was generated as previously described[58]. In brief, 3 mg of W6/32 antibody or 1.5 mg of PdV5.2 antibody was incubated for 1h at room temperature with 1 mL pre-washed protein-A Sepharose 4B packed beads (#101041, Thermo) or protein-G Sepharose 4B packed beads (#101242, Invitrogen), respectively, in glass Econo-columns® (#7374150, Bio-Rad). Each column was washed with 0.2 M sodium tetraborate buffer (pH 9, #B3545, Sigma-Aldrich, Merck) followed by 40 min chemical crosslinking using 20 mM dimethylpimelimidate (#D8388, Sigma-Aldrich, Merck), freshly dissolved in sodium tetraborate buffer. After crosslinking, antibody-bead complexes were washed and incubated for 2 h with 0.2 M ethanol amine (pH 8, #149582500, Thermo), and stored at 4°C in tris-buffer saline (TBS) supplemented with 0.02% sodium azide for up to 3 months. Antibody-bead conjugation and crosslinking was evaluated using Coomassie stain.

Isolation and purification of MHC-I and MHC-II peptides

150-200 mg human brain tissue was homogenized in ice using an IKA basic Ultra-Turrax in freshly prepared lysis buffer containing 1% octyl-β, D-glucopyranoside (OGP) (#O9882, Sigma-Aldrich, Merck), 0.25% sodium deoxycholate (#1065040250, Millipore, Merck), 1.25× cOmplete protease inhibitor cocktail (#4693159001, Roche), 1 mM phenylmethylsulfonyl fluoride (PMSF) (#52332, Sigma-Aldrich, Merck), 0.2 mM iodoacetamide (IAA) (#I1149, Sigma-Aldrich, Merck), and 1 mM ethylenediaminetetraacetic acid (EDTA) (#EDS, Sigma-Aldrich, Merck) in 150 mM NaCl, 50 mM Tris (pH 8). Homogenates were snap-frozen on dry ice, followed by thawing and 1 h incubation on ice while resuspending every 15 minutes. Homogenates were pre-cleared at 3200g at 4 °C for 15 min, followed by a second centrifugation at 20,000g at 4 °C for 30 min. Protein concentrations were determined and normalized using BCA (#23225, Pierce), and lysates were incubated overnight with 200 µL packed protein A:protein G sepharose beads (1:1) in protein LoBind tubes (#0030108450, Eppendorf) on an IKA roller 8 (80 rpm) at 4°C. Pre-cleared lysates were incubated with 200 µL packed MHC-I immunoaffinity resin, pre-washed in TBS, for 1h at 4°C on an IKA roller 8 (80 rpm). Next, the unbound lysate fractions were incubated for 1h with 200 µL pre-washed MHC-II immunoaffinity resin. Resin-bound MHC-peptide complexes were processed further using a Resolvex A200 liquid handling system (Tecan) as earlier described[58]. In brief, captured peptide-MHC complexes were washed ten times with 1 mL TBS, followed by 5 elution steps using 200 µL 10% acetic acid with 5-minute incubation steps. Peptide solid phase extractions were done using Sep-Pak tC18 plates (#186002321, Waters), pre-washed twice in 100% acetonitrile and three times with 0.1% trifluoroacetic acid (TFA). Captured peptides were washed four more times using 0.1% TFA before eluting in 5 times 200 µL 25% ACN 0.1% TFA for MHC-I, and 40% ACN 0.1% TFA for MHC-II. The eluted immunopeptides were transferred to protein LoBind tubes (#0030108450, Eppendorf), vacuum dried and stored at -20 °C until LC-MS/MS injection.

LC-MS/MS analysis

Dried peptides were dissolved in 50 µL 0.1% ACN/0.1% TFA from which 12.5 µL was injected for LC-MS/MS analysis on a UltimateTM 3000 RSLC nanoLC in-line connected to a timsTOF SCP mass spectrometer (Bruker) in case of mouse xenograft samples or in-line connected to

a timsTOF Ultra-2 mass spectrometer in case of human brain samples. Trapping was conducted at a flow rate of 20 µL/min for 2 min in loading solvent A on a 5 mm trapping column (Thermo, Pepmap, 300 µm internal diameter [I.D.], 5 µm beads). The sample was then separated on a reverse-phase column (Aurora elite 75 µm x 150 mm 1.7 µm particles, IonOpticks) following elution from the trapping column. Separation was achieved using a linear gradient, starting at 0.5% MS solvent B (0.1% FA in water/ACN 20:80, v/v) at 250 nL/min for 30 min, increasing to 37.5% MS solvent B, then reaching 55% at 38 min, and further rising to 70% at 40 min. This was followed by the wash for 5 min and re-equilibration with 99.5% MS solvent A (0.1% FA in water). The flow rate was adjusted from 250 nL/min to 100 nL/min at 20 minutes and restored to 250 nL/min at 40 min. A ten PASEF/MSMS scan acquisition method was employed in DDA-PASEF mode with a precursor signals intensity threshold of 500 arbitrary units. Precursors were isolated with a 2 Th window below *m/z* 700 and 3 Th above, with active exclusion for 0.4 min upon reaching a target intensity threshold of 20,000 arbitrary units. In case of MHC-I peptides, an adapted "Thunder" polygon (ref. 38480730) in the *m/z*-IM plane (range 0.7 to 1.25 V s/cm^2) was applied to include HLA-I singly charged precursors, while a broader polygon (range 0.75 to 1.65 V s/cm^2) was used for MHC-II peptides as described previously[58]. The mass spectrometer was operated in non-sensitive mode with an accumulation and ramp time of 100 ms, analyzing in MS from 100 to 1,700 m/z, applying collision energy according to IM range as described[58].

Immunopeptidomics data analysis, binding prediction and visualization

All raw proteomics data were searched using a multi-search engine workflow with follow-up rescoring as described[57]. For human brain samples, the human UniProtKB reference proteome supplemented with the human Aβ1-42 sequence was searched. In case of xenografted mouse samples, a custom protein database consisting of the human and mouse UniProtKB reference proteomes (UP000005640 and UP000000589, respectively) and the human Aβ1-42 sequence. In brief, timsTOF (.d) data was searched by four search engines (MSFragger[77], Comet[78], Sage[79] and PEAKS Studio 12[80] after which search results for each engine were rescored in parallel using TIMS^{2}Rescore[81]. Peptides identified below a 1% peptide q-value were reconciled at the spectrum-level as described[57]. Downstream immuno-informatic analyses included NetMHCpan-4.1[82] and NetMHCIIpan-4.3[83] prediction of binding strength for MHC-I and MHC-II class peptides, respectively, and unsupervised Gibbs clustering[84]. HLA allele information is provided in Supplementary Table 1. Default NetMHCpan %Rank score thresholds were used to define MHC binding strengths.

For functional enrichment analysis of immunopeptides, their corresponding UniProtKB accessions were used. In the case of a peptide matched multiple proteins, the first UniProtKB accession was used as representative. Accessions were entered in the online webtool g:Profiler using default settings[85]. Plots were generated using matplotlib[86] and seaborn[87] in Python (version 3.8.10). Sequence logos were generated using Logomaker[88].

Mice

The *App$^{NL\text{-}G\text{-}F}$* mouse model of amyloidosis contains the humanized Aβ sequence with Swedish (NL), Arctic (G), and Iberian (F) mutations[50]. Control *App$^{hu/hu}$* mice were developed in our lab, and contain the humanised Aβ sequence but no mutations and do not develop plaques[49]. Both strains were crossed with homozygous Rag2tm1.1Flv Csf1tm1(CSF1)Flv Il2rgtm1.1Flv Apptm3.1Tcs mice (Jacksons Lab, strain 017708) to generate *Rag2-/- Il2rγ-/- hCSF1KI App$^{NLG\text{-}F}$* (hereafter referred to as *App^{NLGF}*)and *Rag2-/- Il2rγ-/- hCSF1KI App$^{hu/hu}$* (hereafter *App^{Hu})*. Mice had access to food and water ad libitum and were housed with a 14/10 h light- dark cycle at 21°C in groups of two to five animals. All experiments were reviewed and approved by the

Animal Ethics Committee of KU Leuven (project licenses 177/2017 and 125/2022) in accordance with the European Union Directive 2010/63/ EU.

Microglia xenograft

H9-WA09 ESCs (WiCell Research Institute; RRID:CVCL_9773; with an APOE ε3/ε4 background) and CRISPR-cas9 KO clones (see below) were differentiated into microglial precursors according to the MIGRATE protocol[5,47]. In brief, stem cells were plated and maintained in human Matrigel (Corning) coated 6-well plates and in E8 flex media (Gibco) until reaching ~70-80% confluence. Once confluent, stem cell colonies were dissociated into single cells and plated into U-bottom 96 well plates at a density of ~10k/well in mTeSR1 media with BMP4 (50ng/ml), VEGF (50ng/ml) and SCF (20ng/ml) for 4 days. On day 4, embryoid bodies (EBs) were transferred into 6-well plates (~20 EBs/well) in X-VIVO (+supplements) media supplemented with SCF (50ng/ml), M-CSF (50ng/ml), IL-3 (50ng/ml), FLT3 (50ng/ml) and TPO (5ng/ml) for 7 days, with a full change of media on day 8. On day 11, differentiation media was replaced with X-VIVO (+supplements) with FLT-3 (50ng/ml), M-CSF (50ng/ml) and GM-CSF (25ng/ml). On day 18, human microglial precursors were collected for xenograft. On day 18 of the MIGRATE protocol, microglia precursors were collected and engrafted bilaterally into P4 mouse brains (0.25 million cells per pup per hemisphere) as previously described[5,47]. Before transplantation, mouse microglia were depleted by inhibiting CSF1 receptor (CSF1R) with BLZ945 (dose of 200 mg kg−1) at P2 and P3.

Human microglia isolation from mouse brain - manual method

For CITE-seq experiments, FACs analysis and immunopeptidomics, at the specified ages (described below), xenografted mice were sacrificed using an overdose of sodium pentobarbital followed by transcardial perfusion with 20 ml of ice-cold DPBS (Gibco, Cat #. 14190-144) containing 5 units of heparin (Heparin Leo 25000 IU/5 ml, Leo Pharmaceuticals). The brain omitting cerebellum and olfactory bulb was placed in ice-cold Brain medium buffer (IMDM+glutamax, 2% FBS). The samples were mechanically and enzymatically dissociated in 2mg/ml Collagenase D (Sigma), 1mg/ml Hyaluronidase (Sigma, H3506) and DNase I (Sigma DN25) in brain medium buffer, filtered using a 70 µM strainer (Greiner Bio-One, 542070), washed with 15 ml of ice-cold FACS buffer and centrifuged (300g, 15min, 4°C). Next, a sample clean-up was performed by resuspending the pellet in a 30% isotonic Percoll gradient (Fischer Scientific, cat. #11500744), centrifuging (300g, 15min, 4°C) and removing the layers of myelin and cellular debris that accumulate on top of the sample. The Fc receptors on the cells were blocked in human and mouse FcR blocking solution (1/10, Miltenyi, 130-059-901 and 130-092-575) in ice-cold FACS buffer for 10 min at 4°C. After a 5ml FACS buffer wash and centrifugation (300g, 5 min, 4°C), pelleted cells were incubated in antibodies (described below) for 30 min at 4°C in FACS buffer.

Human microglia isolation from mouse brain – enzymatic method

For scRNAseq and proteomic experiments, at the specified ages (described below), xenografted mice were perfused as described above. One hemisphere was placed in ice-cold FACS buffer (1 × DPBS, 2% FCS and 2 mM EDTA) + 5 µM actinomycin D (ActD; Sigma, Cat. no. A1410-5MG) for dissociation for transcriptomics. Samples were mechanically and enzymatically dissociated using Miltenyi Neural Tissue Dissociation Kit P (Miltenyi, Cat. no. 130-092-628) supplemented with 5 µM ActD. Samples were then passed through a 70-µm strainer (BD Falcon), washed in 15 ml of ice-cold FACS buffer + 5 µM ActD and centrifuged at 300g for 15 min at 4 °C. 5 µM ActD was kept during collection and enzymatic dissociation of the tissue to prevent artificial activation of human microglia during the procedure. ActD was

removed from the myelin removal step to prevent toxicity derived from long-term exposure, and dissociation from that step onwards was as described above for manual dissociation.

Cellular Indexing of Transcriptomes and Epitopes by Sequencing (CITE-seq) on xenografted microglia

6 month *App*^{NLGF} and *App*^{Hu} mice xenografted with APOE e3/e3 microglia[5] (n=3 per strain) were processed for manual dissociation as described above. Cell pellets were incubated for 30 min on ice with antibody mix: PE-Pan-CD11b (1:50, Miltenyi, Cat. no. 130-113-806), BV421-mCD45 (1:500, BD Biosciences, Cat. no. 563890), APC-hCD45 (1:50, BD Biosciences, Cat. no. 555485), and a custom-designed human CITE-Seq antibody panel. The CITE-Seq panel contained 267 unique oligoconjugated antibodies and isotype controls (TotalSeq™-C). Individual mice were tagged and pooled using TotalSeq-C hashtag antibodies. FACS Aria II-sorted single-cell suspensions were resuspended at an estimated final concentration of 1000 cells/µL and loaded on a Chromium GemCode Single Cell Instrument (10× Genomics) to generate single-cell Gel beads-in-EMulsion (GEM). Two DNA libraries were prepared using the GemCode Single Cell 3′ Gel Bead and Library kit, version NextGEM 3.1 (10× Genomics) according to the manufacturer's instructions with the addition of amplification primers (3 nM, 5′CCTTGGCACCCGAGAATT*C*C and 5′GTGACTGGAGTTCAGACGTGTGC*T*C) during cDNA amplification to enrich the TotalSeq-C cell surface protein and hashtag oligos. Size selection with SPRIselect Reagent Kit (Beckman Coulter, B23318) was used to separate amplified cDNA molecules for 3′ gene expression and cell surface protein construction. TotalSeq-A protein library construction including sample index Polymerase Chain Reaction (PCR) using Illumina's Truseq Small RNA primer sets and SPRIselect size selection was performed according to the manufacturer's instructions. The cDNA content of pre-fragmentation and post-sample index PCR samples was analyzed using the 2100 BioAnalyzer (Agilent). Sequencing libraries were loaded on an Illumina NovaSeq flow cell at VIB Nucleomics core with sequencing settings according to the recommendations of 10× Genomics, pooled in an 80:25 ratio for the combined 3′ gene expression and cell surface protein samples, respectively. The Cell Ranger pipeline (10× Genomics, version 6.0.0) was used to perform sample demultiplexing and to generate FASTQ files for read 1, read 2, and the i7 sample index for the gene expression and cell surface protein libraries. Read 2 of the gene expression libraries was mapped to the reference genome (human hg38) using STAR. Subsequent barcode processing, unique molecular identifiers filtering, and gene counting was performed using the Cell Ranger suite version 6.0.0 (10× Genomics) and Seurat v4.0.5. For further analysis, we used the filtered featurebarcode matrix generated by CellRanger (v6.0.0, 10× Genomics).

CITE-seq preprocessing and macrophage identification for exclusion

Raw CITE-seq data were first processed in Seurat to perform initial quality control and to identify macrophages for exclusion from downstream microglia-focused analyses. Cells were filtered using standard single-cell quality control metrics, including total UMI counts, number of detected genes, and the fraction of mitochondrial reads. Then, RNA counts were normalized and variance-stabilized using SCTransform. To mitigate batch-associated technical variation, Harmony was applied to the SCTransform-derived low-dimensional representation (PCA on SCT residuals), using sample annotations as integration variables. The Harmony-corrected embeddings were then used to construct a shared nearest neighbor (SNN) graph, followed by graph-based clustering and UMAP visualization. Macrophages were identified based on canonical macrophage marker expression and cluster-level marker enrichment. The cell barcodes corresponding to these macrophage clusters were extracted and used as an exclusion list for subsequent analyses. The remaining cells were treated as the microglia compartment. Microglia clusters were subsequently annotated into microglia cell states using

RNA markers by comparing cluster-specific differentially expressed genes with curated microglia marker gene lists[5].

Scoring of antigen presentation and visualization on RNA embeddings

To quantify antigen presentation activity at single-cell resolution, the raw count matrices were additionally imported into Scanpy. Cells annotated as macrophages in the Seurat analysis were removed by matching Seurat-derived macrophage barcodes to the AnnData cell index, thereby restricting downstream analyses to microglia as defined above. Denoised ADT values were obtained using totalVI[89]. totalVI was trained on the macrophage-depleted dataset to model CITE-seq technical noise and protein background, and posterior denoised protein abundance estimates were extracted. These denoised protein values were used for downstream scoring analyses. An antigen presentation (APC) score was then computed per cell using Scanpy's score_genes function, applied to a curated set of antigen presentation–associated features. In Scanpy, score_genes summarizes the expression of a target feature set in each cell relative to matched control features, producing a per-cell module score. The resulting APC score was stored as cell-level metadata, and cells with scores in the top 10% of the microglia distribution (≥ 90th percentile) were labeled as APC-positive. Finally, APC scores and APC-positive labels were visualized by projecting them onto the RNA-based UMAP embedding, enabling interpretation of antigen presentation activity in the context of RNA-defined microglia cell states. To compare antigen presentation activity between genotypes, we aggregated APC scores at the mouse level. Specifically, for each mouse (3 WT and 3 AD), we calculated the mean APC score across all microglia profiled from that individual, yielding one value per mouse. Group differences in mouse-level mean APC score were then assessed using a two-sided unpaired Student's t-test comparing WT versus AD mice, with $P < 0.05$ set as significant.

Immunopeptidomics on xenografted microglia

12M *App*^{NLGF} mice xenografted with H9 human microglia progenitors were sacrificed using an overdose of sodium pentobarbital followed by transcardial perfusion with 20 ml of ice-cold DPBS (Gibco, Cat #. 14190-144) containing 5 units of heparin (Heparin Leo 25000 IU/5 ml, Leo Pharmaceuticals). For immunopeptidomics on total brain (n=1), the brain omitting cerebellum and olfactory was immediately snap frozen on dry ice. For immunopeptidomics on pre-sorted human microglia, the sample was processed as detailed above (Human microglia isolation from mouse brain by manual methods). After Fc block and FACS buffer wash and centrifugation (300g, 5 min, 4°C), pelleted cells were incubated for 30 min at 4°C in FACS buffer with the viability dye eFluor780 (1/2000; Thermo Fisher Scientific, 65-0865-14) and the following antibodies: PE pan CD11b (1/50; Miltenyi, 130-113-806), APC human CD45 (1/50; BD Biosciences, 555485), BV421 mouse CD45 (1/500; BD Biosciences, 563890). Following incubation, cells were washed, pelleted through centrifugation (300g, 5 min, 4°C), resuspended in 500 µl ice-cold FACS buffer and passed through a 35 µm strainer, before sorting on the MACSQuant Tyto. Human microglia were considered positive for CD11b and hCD45 and 600,000 cells were sorted, pelleted, washed in DPBS and snap frozen. Both total brain and pre-sorted samples were processed as described above for human brain samples ("Immunopeptidomics") and as in[58], with the following deviations: pre-sorted human microglia cells were lysed in 100 µL lysis buffer, and HLA-I and -II immunopeptide isolation and purification were also performed in 96-well plate format using the Tecan Resolvex A200. Mass Spectrometry and data analysis was performed as described above.

Generation of CRISPR-cas9 KO lines

H9 ESCs were culturing with the Cellartis DEF-CS 500 Culture System (Takara; #Y30010 & #Y30017). Cells were kept in a humidified chamber at 37°C with 5% CO_2. CRISPR/Cas9

genome editing was utilized to generate bi-allelic knockouts (KO) for the PICALM gene. Guide RNAs were designed using crispor.tefor.net, which identifies and ranks guide RNAs based on input sequences, considering on-target and off-target activity. Guides were selected for high specificity and for targeting regions that cover all potential splice variants of the gene. A two-guide strategy was employed to maximize KO efficiency. The guides (Table 1) were delivered as RNP complexes (IDT, Leuven, Belgium) via electroporation using the NEPA21 electroporator (Nepagene). Electroporated hESCs were plated at a density of 100K cells/cm² and allowed to recover for 72 hours. After recovery, the cells were divided into two fractions: one for assessing CRISPR/Cas9 gene editing efficiency via PCR, and the other for single-clones expansion in a 96-well plate. Once CRISPR/Cas9 gene editing was confirmed in the first fraction, single clones were expanded and checked for bi-allelic editing via Sanger sequencing. Two independent clones (further referred to as cl.1(P1.22); cl.2(P7E7)) were chosen carrying a deletion in both alleles. Confirmation of knock-out efficiency was done by measuring protein expression using western blot. All clones were checked for chromosomal abnormalities using a Microarray-based Comparative Genomic Hybridization (CGH) assay at the Centre for Human Genetics (Gasthuisberg, UZ Leuven) and tested for mycoplasma. The pluripotent stem cell characteristics of the clones were confirmed through qPCR and immunohistochemistry of stem cell markers (data not shown).

Table 1: sequences of guides and specificity score.

guide	Sequence (5' → 3')	PAM	Specificity score
PICALM exon 6	GTCTAATGGCATCTTTGAAC	AGG	81
PICALM intron 6/7	AAGTAACGTGGACTTACTCA	GGG	84
PICALM exon 11	CCCTAGTTCTTCTAACAGGT	AGG	87

Table 2: antibodies used in WB.

antibodies	Host	Dilution WB	Catalogue #	Company
PICALM (EPR12177)	Rabbit	1:1000	ab172962	Abcam
Beta actin	Mouse	1:20000	A5441	Sigma
Goat anti mouse HRP	Goat	1:10000	170-6516	Biorad
Goat anti rabbit HRP	Goat	1:10000	170-6515	Biorad

Isolation of human microglia for single-cell transcriptomics and proteomics

Samples were obtained at 6 months post-transplantation from App^{NLGF} and App^{Hu} mice xenotransplanted with H9 or $PICALM^{-/-}$ microglia. After enzymatic dissociation (above), pelleted cells were incubated with the following antibodies: PE-Pan-CD11b (1:50, Miltenyi, Cat. no. 130-113-806), BV421-mCD45 (1:500, BD Biosciences, Cat. no. 563890), APC-hCD45 (1:50, BD Biosciences, Cat. no. 555485), Total-Seq A cell hashing antibodies (1:500, BioLegend) and viability dye (1:2,000, eFluor 780, Thermo Fisher Scientific, Cat. no. 65-0865-14), in cold FACS buffer for 30 min at 4 °C. After incubation, cells were washed, and the pellet was resuspended in 600 µl of FACS buffer and passed through a 35-µm strainer before sorting. For sorting, the cell suspension was loaded into the input chamber of a MACSQuant Tyto Cartridge and human cells were sorted based on CD11b and hCD45 expression at 4 °C. Per mouse 40,000 cells were sorted for scRNAseq, followed by a second sort to obtain 100,000 cells from proteomics. FACS data were analyzed using FlowJo v10.8.1.

Single-cell library preparation and sequencing

Sorted cells were diluted to a final concentration of 1000 cells/µl. Since all the samples were individually hashed using TotalSeq™-A cell hashing antibodies, for each mouse strain ((*App*^{NLGF} and *App*^{hu}) 18,000 human microglia/animal were pooled and 3 separate libraries loaded onto the Chromium Next GEM Chip G (PN #2000177) (*App*^{NLGF}) or onto the Hydrop[90] (*App*^{hu}). The DNA library preparations were generated following manufacturers' instructions (CG000204 Chromium Next GEM Single Cell 3' Reagent Kits v3.1). In parallel, the hashtag oligo libraries were prepared according to manufacturers' instructions (BioLegend - TotalSeq™-A Antibodies and Cell Hashing with 10x Single Cell 3' Reagent Kit v3 3.1 Protocol) using 16 cycles for the index PCR. A total of 6 libraries (3 libraries *App*^{NLGF}, 3 libraries *App*^{hu}) containing biological replicates (n=5-6 per genotype per strain) were sequenced targeting 90% mRNA and 10% hashtag oligo library (55,000 reads/cell) on a HiSeq4000 or NovaSeq6000 (Illumina) platform with the recommended read lengths by 10X Genomics workflow.

Analysis of single-cell RNA sequencing data

Alignment and quality control

Each library was processed as follows: Cellranger v6.0.1 was used to demultiplex oligo-tagged antibodies and align sequencing output to a combined human and mouse reference genome (assemblies hg38 and mm10). Down-stream analysis was performed using the Seurat v4.2.0 package (v4.2.1)[91,92]. To align samples to barcodes, we normalised the hash count matrix using a centered log ratio (CLR), then demultiplexed the data using HTODemux with default settings. We used the demultiplexed data to remove negatives (cells that were not assigned a barcode) and doublets (cells that were assigned more than one barcode) as well as cells with a mitochondrial percentage above 10% or more than 250 mouse reads. For the RNA count matrix (after removing genes aligned to the mm10 mouse reference), we filtered out cells with gene counts below 300, or above 3000. Additionally, we removed cells belonging to proliferating and macrophage clusters, before re-clustering.

Normalisation and integration

Raw counts from all libraries were normalized SCTransform[93] using the "glmGamPoi" method, retaining the 10.000 most variable features for downstream analysis. Following Principal Component Analysis (PCA), the first 20 principal components were retained based on visual inspection of the scree plot. To mitigate biological and technical batch effects, data were integrated using Harmony[94] with 'Library' and 'Mouse' as co-variates. We then calculated nearest neighbors and Uniform Manifold Approximation and Projection (UMAP) coordinates using the integrated harmony components.

WGCNA and module identification

Co-expression network analysis was performed using the WGCNA R package to identify modules of highly correlated genes. The top 5,000 variable genes were selected from the dataset. Network construction was performed on SCT's pearson residuals gene expression matrix. A signed gene co-expression network was constructed using the `blockwiseModules` function. A soft-thresholding power of 10 was selected based on the scale-free topology fit index. Modules were detected using a minimum module size of 4 genes, a deep split parameter of 2, and a merge cut height of 0.999. Module eigen-genes (MEs), representing the first principal component of the expression matrix for each module, were calculated to quantify module expression profiles across cells.

Differential expression and pathway analysis

Differential expression (DE) was performed using a pseudo-bulk approach. Raw counts were aggregated across mouse and cell state. DE analysis was performed using the DESeq2

package for R, v.1.36.0. Briefly, data was normalized using a median-of-ratios method, and a variance-stabilizing transform performed to reduce over-dispersion. Then a negative binomial model was fit, and genes were tested for differential expression using a Wald test. P-values were corrected using a Benjamini-Hochberg correction. DE was performed using H9 as a control vs *PICALM*$^{-/-}$, in *App*^{NLGF} and *App*^{Hu} separately.

Differential expression and pathway analysis

Functional enrichment analysis was performed using the fgsea R package. Genes were ranked based on their log2 fold change values obtained from the differential expression analysis. Enrichment was tested against gene sets from the GO Biological Processes and KEGG MEDICUS databases. Additionally, over-representation analysis was used to test for the enrichment of biological pathways within our WGCNA modules, to aid in their identification.

Proteomics

Proteomics Sample Preparation

For proteomics, 100,000 human microglia (CD11b+, hCD45+) from each mouse (n=5 *App*^{Hu}-H9 & *App*^{Hu}-*PICALM*$^{-/-}$; n=6 *App*^{NLGF} -H9 & *App*^{NLGF}-*PICALM*$^{-/-}$) were sorted on the MACSQuant Tyto. Collected microglia were washed 2 x in DPBS and centrifuged to remove FBS contaminants from FACS buffer, and pelleted cells were snap frozen. All samples were lysed in 50µl lysis buffer (5% SDS, 10mM TCEP, 50mM TEAB) and shaken at RT for 5 minutes at 1000rpm, followed by boiling at 95°C for 5 minutes at 500rpm. Samples were then shaken again at RT for 5 minutes at 1000rpm before being sonicated for 15 cycles of 30 seconds on/ 30 seconds off with a BioRuptor (Diagenode). Benzonase was added to each sample and incubated at 37°C for 15 minutes to digest DNA. Samples were then alkylated with 20mM iodoacetamide for 1 hour at 22°C. Protein concentration was determined using EZQ protein quantitation kit (Invitrogen) as per manufacturer instructions. Protein isolation and clean up was performed using S-TRAP™ (Protifi) columns before digestion with trypsin at 1:20 ratio (enzyme:protein) for 2 hours at 47°C. Digested peptides were eluted from S-TRAP™ columns using 50mM ammonium bicarbonate, followed by 0.2% aqueous formic acid and 50% aqueous acetonitrile containing 0.2% formic acid. Eluted peptides were dried down overnight.

Mass Spectrometry

Dried peptides were rehydrated in 210µl 5% formic acid, shaking at 1000rpm for 1 hour at 30°C ready for injection onto the Orbitrap Exploris (Thermo Fisher) mass spectrometer using data independent acquisition (DIA). Peptides (2 µg/ sample) were injected onto a nanoscale C18 reverse-phase chromatography system (UltiMate 3000 RSLC nano, Thermo Scientific) and electrosprayed into an Orbitrap Exploris Mass Spectrometer (Thermo Fisher). For liquid chromatography the following buffers were used: buffer A (0.1% formic acid in Milli-Q water (v/v)) and buffer B (80% acetonitrile and 0.1% formic acid in Milli-Q water (v/v). Samples were loaded at 10 µL/min onto a trap column (100 µm × 2 cm, PepMap nanoViper C18 column, 5 µm, 100 Å, Thermo Scientific) equilibrated in 0.1% trifluoroacetic acid (TFA). The trap column was washed for 3 min at the same flow rate with 0.1% TFA then switched in-line with a Thermo Scientific resolving C18 column (75 µm × 50 cm, PepMap RSLC C18 column, 2 µm, 100 Å). Peptides were eluted from the column at a constant flow rate of 300 nl/min with a linear gradient from 3% buffer B to 6% buffer B in 5 min, then from 6% buffer B to 35% buffer B in 115 min, and finally to 80% buffer B within 7 min. The column was then washed with 80% buffer B for 4 min and re-equilibrated in 3% buffer B for 15 min. Two blanks were run between each sample to reduce carry-over. The column was kept at a constant temperature of 50°C. The data was acquired using an easy spray source operated in positive mode with spray voltage at 2.445 kV, and the ion transfer tube temperature at 250°C. The MS was operated in DIA mode. A scan

cycle comprised a full MS scan (m/z range from 350-1650), with RF lens at 40%, AGC target set to custom, normalized AGC target at 300, maximum injection time mode set to custom, maximum injection time at 20 ms, microscan set to 1, and source fragmentation disabled. MS survey scan was followed by MS/MS DIA scan events using the following parameters: multiplex ions set to false, collision energy mode set to stepped, collision energy type set to normalized, HCD collision energies set to 25.5, 27 and 30 %, orbitrap resolution 30000, first mass 200, RF lens 40 %, AGC target set to custom, normalized AGC target 3000 %, microscan set to1, maximum injection time 55 ms. Data for both MS Scan and MS/MS DIA Scan events were acquired in profile mode. Resultant mass spectra files were analysed using DIA-NN v.1.8.1 using the library free method using a human FASTA file (Uniprot, downloaded August 2023) along with the additional contaminants FASTA. The default parameters were used except for "Heuristic protein inference" and the protein inference was set to use the protein names from the FASTAs. A single-pass neural network classifier was used with no MBR.

Proteomics data analysis

Initial data filtering was performed, removing non-uniquely mapping peptides as well as common contaminants (cross-reference with the cRAP repository (https://www.thegpm.org/crap/index.html)). Given that samples derived from App^{Hu} and App^{NLGF} mice were processed separately, comparison of the H9 vs *PICALM* KO data were also performed per strain. Proteins that had a missing value (NA) for 5/10 (App^{Hu}) or 5/11 (App^{NLGF}) samples or more were discarded from the analysis. Following quantile normalization and log2 transformation, differential expression analysis was performed in R (v.4.3.2) using limma (v.3.58.1) comparing H9 vs $PICALM^{-/-}$ per strain while correcting for processing batch effects (date of sacrifice), with Benjamini-Hochberg FDR (false discovery rate) set at padj<0.05.

Histology

At the time of collecting mouse brains for transcriptomics and proteomics (6 months, see above), one hemisphere was preserved and postfixed in 4% PFA overnight at 4 °C. After 24 h, PFA was removed, brains washed and stored in 1 × DPBS with 0.01% NaN3 at 4 °C until further processing. For sectioning, brains were cut coronally (40-µM thickness) with a vibrating microtome (Leica). Each sample was collected under free-floating conditions in a series of six sections spanning the entire rostra-caudal axis and stored in cryoprotectant solution (40% PBS, 30% ethylene glycol, 30% glycerol) at −20 °C. For staining, sections were washed in 1 × DPBS and permeabilized for 15 min at room temperature in PBS with 0.2% Triton. For sections labelled with X34 stain: after permeabilization, sections were stained with X-34 staining solution (10 µM X-34 (Sigma-Aldrich), 20 mM NaOH (Sigma-Aldrich) and 40% ethanol) for 20 min at room temperature. Sections were washed several times with 40% ethanol for 2 min and with PBS + 0.2% Triton for 5 min. All sections were blocked with 5% normal donkey serum or 5% normal goat serum (depending on secondary antibodies) in PBS + 0.2% Triton for 1 h at room temperature, and incubated with primary antibodies in blocking solution overnight at 4 °C. Primary antibodies and dilutions were: HLA-DR/DP/DQ (CR3/43, ab7856, Abcam, 1:200), P2RY12 (Atlas Antibodies cat.# HPA014518, 1/1000) IFITM3 (Cell Signaling, 59212, 1:300), human nuclei (Millipore MAB1281 1:1200). For IFITM3, signal was enhanced using a Tyramide SuperBoost kit (B40915, Thermo fisher) according to the manufacturer's instructions. Briefly, after overnight incubation with primary antibody, sections were incubated with a poly-HRP-conjugated secondary antibody. Tyramid solution was then added to the slices for 5 min and they were washed in PBS after the reaction was stopped. Secondary antibodies were incubated for 2 h at room temperature in blocking solution. After washing, sections were mounted in Glycergel mounting medium (C0563 DAKO). Images at 4x (IFITM3) or 40x (HLA-DR) magnification were taken on Nikon A1R Eclipse and Nikon AX confocal microscopes. Areas for imaging and analysis of HLA-DR were selected

blindly based on 2 criteria: human P2RY12 expression (engraftment) and x34 plaque load. Quantification was performed in Imaris v10 (Oxford Instruments) using an automated analysis protocol.

FACS analysis of human xenografted microglia

Microglia were isolated from 6 month xenografted mice and processed as described above (Manual digestion). Antibodies used for staining were: viability with eF780 dye (Thermo Fischer, cat. #65-0865-18), Alexa Fluor 488 anti-human CD45 (cat. #304017, Biolegend); PE/Dazzle 594 anti-human CD274 (PD-L1; cat. #329732, Biolegend)); PeCy7 anti-human HLA-DR (cat. #307616, Biolegend); Brilliant Violet 421 anti-human CD80 (cat. #305221, Biolegend); PE anti-human CD86 (cat. #305438, Biolegend); APC anti-human HLA A/B/C (cat. #307616, Biolegend), PerCP/Cyanine5.5 anti-human CD40 (clone 5C3, cat. 334315, Biolegend). Precision Counting beads (cat. #424902, Biolegend) were added before acquisition. Samples were acquired and counted on a BD FACSymphony A1 (BD Biosciences) and analyzed using FlowJo v10.8.1 (BD Biosciences). Human microglia were gated based on human CD45 expression and this population was then gated for expression of all other markers.

***In vivo* phagocytosis assays**

At 10 months of age, App^{NLGF} mice xenotransplanted with H9 and $PICALM^{-/-}$ cl.1 were injected i.p. with 10mg/kg of methoxy-X04 (Tocris #4920), reconstituted in Kolliphor-EL (Sigma #C5125; protocol adapted from[95]). Three hours after methoxy-X04 injection, mice were euthanized, perfused and brains dissociated with enzymatic method as described above. Cells were washed in 5 ml of FACS buffer and pelleted cells were incubated with the following antibodies: PE-Pan-CD11b (1:50, Miltenyi, Cat. no. 130-113-806), AF488-mCD45 (1:500, Biolegend Cat. no. 109815), APC-hCD45 (1:50, BD Biosciences, Cat. no. 555485), PE-Cy7 HLA-DR/DQ/DP (1:80) and viability dye (1:2,000, eFluor 780, Thermo Fisher Scientific, Cat. no. 65-0865-14), in cold FACS buffer for 45 min at 4 °C. After incubation, cells were washed and fixed with eBioscience Foxp3 Fixation/Permeabilization kit (eBioscience Cat. No. 00-5521-00) for 30 min at 4 °C. For intracellular CD68 staining, fixed cells were permeabilized (eBioscience Cat. no. 00-8333-56), washed and incubated in PE Vio615 CD68 (1/100 Miltenyi Cat. No. 130-114-656) in permeabilization buffer overnight at 4 °C. Cells were washed with FACS buffer, the pellet was resuspended in 500 µl of FACS buffer and passed through a 35-µm strainer prior to FACS acquisition. Flow data was acquired on a BD FACSCanto II. Dead cells and doublets were gated out prior to downstream analysis. Human microglia were identified by gating on hCD45. Methoxy-X04 gating was set with negative controls (xenografted App^{Hu} mice injected with methoxy-X04). Methoxy-X04 populations within the hCD45 and within the CD68-positive gate were analysed for methoxy-X04 incorporation. FACS data was analysed with FlowJo software (v10.8.1).

Methoxy-sequencing

At 9-10 months of age, methoxy-X04 treatment and brain sample preparation was performed as described above, with the following modifications. Cells were incubated with following antibodies: PE-Pan-CD11b (1:50, Miltenyi, Cat. no. 130-113-806), AF488-mCD45 (1:500, Biolegend Cat. no. 109815), APC-hCD45 (1:50, BD Biosciences, Cat. no. 555485) and viability dye (1:2,000, eFluor 780, Thermo Fisher Scientific, Cat. no. 65-0865-14), in cold FACS buffer for 30 min at 4 °C. Cells were washed with FACS buffer, the pellet was resuspended in 600 µl of FACS buffer and passed through a 35-µm strainer prior to FACS acquisition. For sorting, the cell suspension was loaded into the input chamber of a MACSQuant Tyto Cartridge. Cells were sorted on the MACSQuant Tyto at 4 °C, with dead cells gated out (e780+) before human

microglia (CD11b+, hCD45+) were sorted based on either methoxy-X04 (BV421 channel) positive gate or methoxy-X04 negative gating. Methoxy-x04 gating was set with negative controls (xenografted *App*^{Hu} mice injected with methoxy-X04). 5,000 methoxy-X04 positive cells and 5,000 methoxy-X04 negative cells were sorted out from each mouse. Samples were washed once with DPBS, pelleted at 1000g, pellets snap frozen and stored at -80°C.

Sequencing and data analysis

For bulk RNAseq analysis, RNA extraction was performed with Qiagen RNeasy micro extraction kit. RNA concentration and purity were determined with a Bioanalyzer 2100 (Agilent Technologies), and 1ng of total RNA per sample was used as input for the Smart-Seq Stranded Library protocol to generate full-length cDNA. Sequence-libraries of each sample were finally equimolarly pooled and sequenced on an Element Bio AVITI instrument using AVITI 2 × 75 Cloudbreak Freestyle High sequencing kit single-end reads (101–8-8–0), 1% PhiX, at the VIB Nucleomics Core (www.nucleomics.be). Reads were aligned against a combined human GRCh38 and murine mm10 reference to allow species disambiguation using STAR. PCR/optical duplicates were subsequently removed from the sorted BAM files with Picard MarkDuplicates. Gene-level read counts on the deduplicated alignments were then re-computed using featureCounts. Counts were imported into R and split by species. For each sample, the fraction of reads mapping to mouse versus human was computed as `mouse / (mouse + human)` and used as a quality metric. Only the human (GRCh38) counts were retained for downstream expression analyses. Genes with fewer than 100 counts across all samples were removed prior to model fitting. Differential expression was performed with DESeq2. A model of the form “~ MeX04 + ID” was fit separately to the H9 control and PICALM KO samples, to evaluate genotype-specific phagocytic-state responses. P-values were adjusted using the Benjamini–Hochberg (FDR) method. Final-figure plots were produced with ggplot2 using a colour-blind-friendly palette derived from the khroma library.

Statistics

For data visualisation and statistics not already described above, statistical analyses and data visualization were performed using GraphPad Prism (v10). Data are presented as scatter dot plot with bar, and the line at the mean ± s.e.m. (standard error of the mean). All n values represent individual animals. To avoid litter bias in the mouse experiments, experimental groups were composed of animals from different litters randomly distributed. Analyses were conducted with automated analysis pipelines. Comparisons between two groups following a normal distribution were analyzed using two-tailed unpaired t-test, while comparisons between two groups not following a normal distribution were analyzed using the Mann–Whitney test. The statistical tests are reported in the figure legends and for all analyses, $\alpha = 0.05$.

Supplementary Files

This is a list of supplementary files associated with this preprint. Click to download.

- Borriesupplementarytables.xlsx